Dickinson) with a small amount of RPMI-1640. These cells were centrifuged, resuspended, and concentrated to 1×10^6 VX2 cells/ml. Then, 2 ml of the solution was simultaneously injected into the thigh muscle of two rabbits; one rabbit was used for successive transplantation, and the other rabbit was used for survival analysis. Following this protocol, the same experimental procedure was repeated three times at 3-week intervals. To compare the morphological and biological properties of the EGFP gene-introduced VX2 transplantation model with those of the conventional VX2 transplantation model, we performed conventional VX2 transplantations in parallel using the same source of VX2 cells as shown in Fig. 1.

Macroscopic imaging of EGFP gene-introduced VX2 tissue

A light-emitting diode irradiation device for GFP observation (LEDGFP-WCCT; Optcode; Tokyo, Japan) and an IVIS Lumina II Imaging System (Summit Pharmaceuticals International; Tokyo, Japan) were used for the gross observation of EGFP gene-introduced VX2 cancer tissue.

Microscopic study of EGFP gene-introduced VX2 cells

To compare EGFP gene-introduced VX2 cancer cells and conventional VX2 cancer cells, microscopic studies were performed as follows. For the cytological study, cells were obtained by scratching from the cut surfaces of VX2 cancer tissue and were then imprinted onto silane-coated glass slides (Silane S; Muto Pure Chemicals; Tokyo, Japan) for each successive transplantation. These glass slide samples were immediately fixed in 98 % ethanol, and then Papanicolaou stain was performed on them.

For histopathological studies, VX2 cancer tissue was fixed in 20 % neutral buffered formalin and embedded in paraffin. An immunohistochemical study was performed on

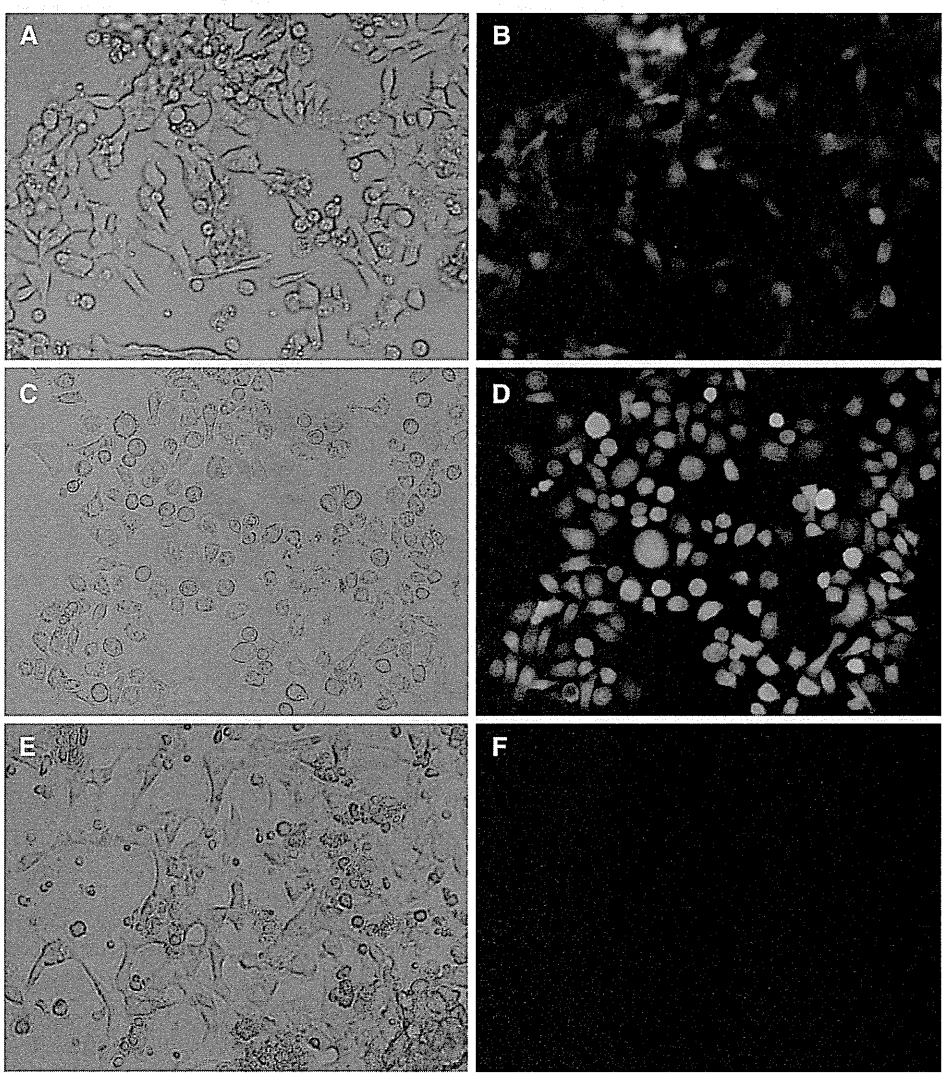

Fig. 2 EGFP gene-introduced VX2 cancer cells at day 9 in the primary culture dish demonstrating green fluorescent protein (GFP) expression (**a** phase contrast light microscopy, objective 40×. **b** Fluorescence microscopy, objective 40×). EGFP gene-introduced VX2 cancer cells at day 4 in the secondary culture dish demonstrating GFP expression (**c** phase contrast light microscopy, objective 40×. **d** Fluorescence microscopy, objective 40×). Conventional VX cancer cells at day 9 in the primary culture dish demonstrating no GFP expression (**e** phase contrast light microscopy, objective 40×. **f** Fluorescence microscopy, objective 40×)

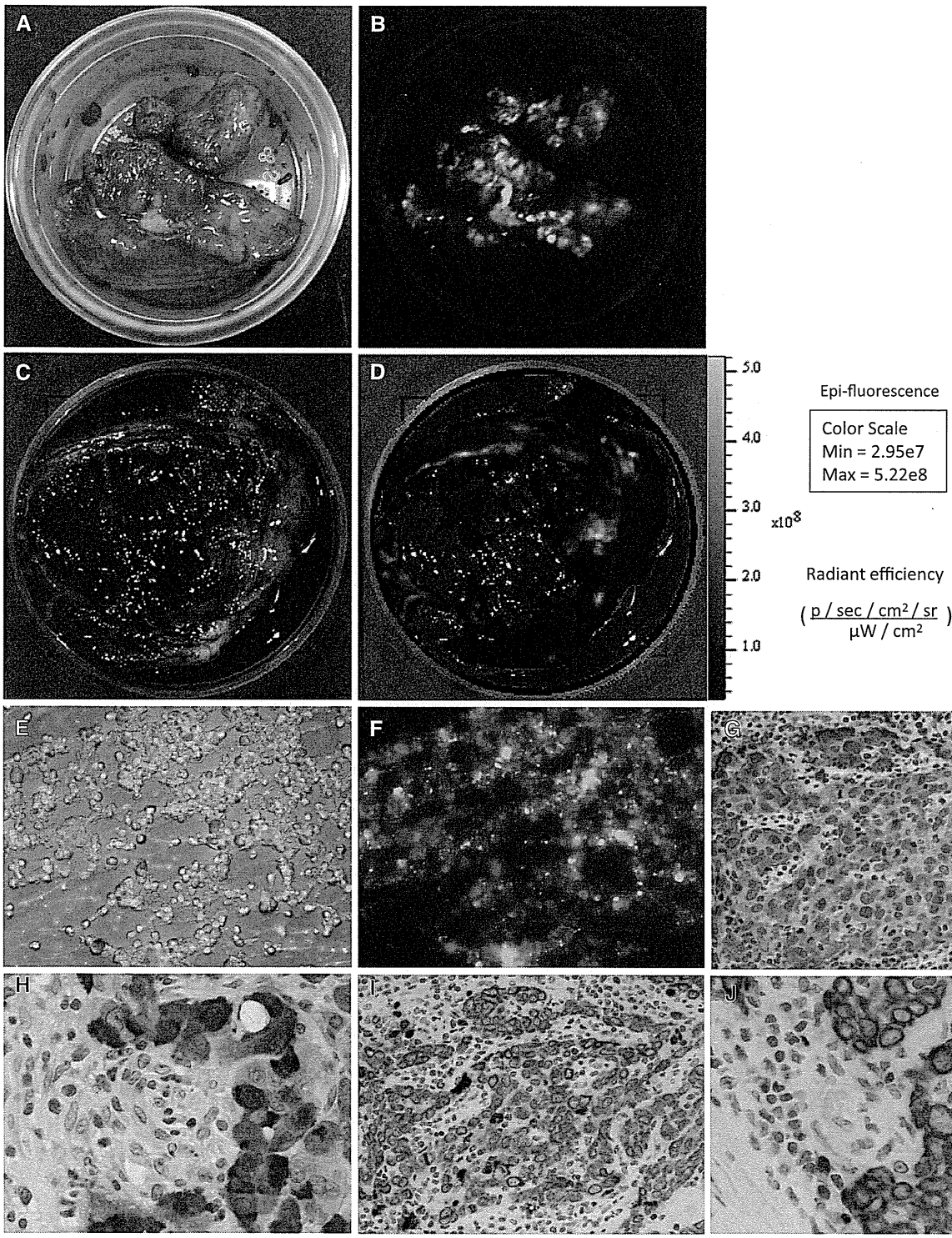

VX2 cancer tissue using antibodies against Ki-67 (MIB-1; Dako Japan; Tokyo, Japan), GFP (sc-101525; Santa Cruz; Dallas, Texas, The United States), pan-cytokeratin (AE1/AE3; Dako Japan), vimentin (V9; Dako Japan) and an antibody detection kit (Histofine Simple Stain MAX PO (M); Nichirei Bioscience; Tokyo, Japan), according to the manufacturer's instructions. Hematoxylin and eosin stain and immunohistochemical stain were used for distinguishing VX2 cells from stromal cells. The slide evaluation was performed by independent board-certified pathologists,

◀**Fig. 3** Green fluorescent protein (GFP) expression in EGFP gene-introduced VX2 cancer cells that were transplanted and grown in the thigh muscles of rabbits. **a** The gross picture of EGFP gene-introduced VX2 showing a solid growth. **b** The gross picture corresponding to **a** demonstrating GFP expression (illuminated by the light-emitting diode irradiation device and visualized with the GFP observation filter). **c** The gross picture of EGFP gene-introduced VX2 showing cystic degeneration. **d** The gross picture corresponding to **c** demonstrating GFP expression (captured by IVIS). **e** The photomicrograph of a scratch cytological sample obtained from the cut surfaces of EGFP gene-introduced VX2 cancer tissues (98 % ethanol-fixed, unstained sample, under a light microscope, objective 40×). **f** The photomicrograph corresponding to **e** demonstrating that VX2 cancer cells express green fluorescence (98 % ethanol-fixed, unstained sample, under a fluorescent microscope, objective 40×). **g** The photomicrograph of EGFP gene-introduced VX2 cancer tissue demonstrates that VX2 cancer cells positive for GFP (immunohistochemistry, objective 40×). **h** The photomicrograph of EGFP gene-introduced VX2 cancer tissue demonstrates that VX2 cancer cells are positive for GFP, whereas non-neoplastic stromal cells are negative for GFP (immunohistochemistry, objective 40×, magnified 2×). **i** The photomicrograph of EGFP gene-introduced VX2 cancer tissue demonstrates that VX2 cancer cells are positive for pan-cytokeratins (AE1/AE3) (immunohistochemistry, objective 40×). **j** The photomicrograph of EGFP gene-introduced VX2 cancer tissue demonstrates that VX2 cancer cells are positive for pan-cytokeratins (AE1/AE3), whereas non-neoplastic stromal cells are negative for pan-cytokeratins (AE1/AE3) (immunohistochemistry, objective 40×, magnified 2×)

and the positive rates in VX2 cells and stromal cells against these antibodies were, respectively, calculated by counting approximately 1,000 cells at randomly selected high power fields under the light microscope. In addition, specificity of EGFP expression in VX2 cells was investigated by these slides.

For transmission electron microscopy, VX2 cancer tissue specimens were fixed in 2.5 % glutaraldehyde at 4 °C overnight and were then fixed with 1 % osmium tetroxide in 0.1 M PBS (pH 7.4) for 2 h at room temperature and washed with PBS. Following dehydration using a graded series of ethanol solutions, the tumor samples were infiltrated with propylene oxide and embedded in an epoxy resin (Plain Resin Kit; Nisshin EM; Tokyo, Japan). Ultrathin sections were stained with uranyl acetate for 20 min and then with lead nitrate for 10 min. The sections were then examined by transmission electron microscopy (H-7500; Hitachi; Tokyo, Japan). Independent board-certified pathologists evaluated the electron microscopic images in a blinded manner.

Statistical analysis

The weights and ages of the rabbits at the time of transplantation, the longest diameter of the tumors 3 weeks after transplantation and the Ki-67 labeling indices of the tumors were compared between the EGFP gene-introduced VX2 rabbit group and the conventional VX2 rabbit group using an unpaired Student's t test if the normal distribution was assumed or the Mann–Whitney U test if a normal distribution was not assumed. The Kolmogorov–Smirnov test and the Shapiro–Wilk test were used to evaluate the normality of the variables. Levene's test was used to evaluate the equality of the variance. For comparison of the survival rates between the conventional VX2 rabbit group and the EGFP gene-introduced VX2 rabbit group, the Kaplan–Meier method and the log-rank test were used. All P values were calculated using two-tailed tests, and those values <0.05 were considered statistically significant. These statistical analyses were performed using the SPSS 18.0 J software (IBM SPSS; Tokyo, Japan).

Results

In vitro culture findings of EGFP gene-introduced and conventional VX2 cancer cells

In the gene transfer study, EGFP expression was observed at 70.5 % of VX2 cells in the primary culture and 95.0 % in the secondary culture (Fig 2a–d). However, cultured conventional VX2 cells did not express EGFP (Fig. 2e, f).

Transplantation findings of EGFP gene-introduced and conventional VX2 cancer cells

Serial transplantation study of EGFP gene-introduced VX2 cells and conventional VX2 cells exhibited a success rate of 100 % (8/8) in both groups. The mock transfection control study exhibited no tumor growth 16 weeks after transplantation, and the cultured VX2 transplantation control study demonstrated tumor growth 3 weeks after transplantation. Grossly, the tumors grown in the thigh showed expansive growth with a varying degree of cystic degeneration in both groups. Using a light-emitting diode irradiation device and IVIS, expression of green fluorescence was observed only in the EGFP gene-introduced group corresponding to cancer tissues (Fig. 3a–d).

Scratch cytological samples obtained from the cut surface of EGFP gene-introduced VX2 cancer tissues exhibited green fluorescence under the fluorescence microscope (Fig. 3e, f). In formalin-fixed, paraffin-embedded tissue samples obtained from the EGFP gene-introduced VX2 group, the positive rates in VX2 cancer cells for GFP, pan-cytokeratin and vimentin were 84.3 ± 1.1 % (mean ± SE; range 78.8–88.9), 100.0 ± 0 % (mean ± SE) and 1.08 ± 0.20 % (mean ± SE; range 0.37–2.13), respectively; whereas fibroblasts, lymphocytes and endothelial cells in this group were all positive for vimentin at 100 % level, and these stromal cells were entirely negative for GFP (Fig. 3g–i). On the other hand, in formalin-fixed,

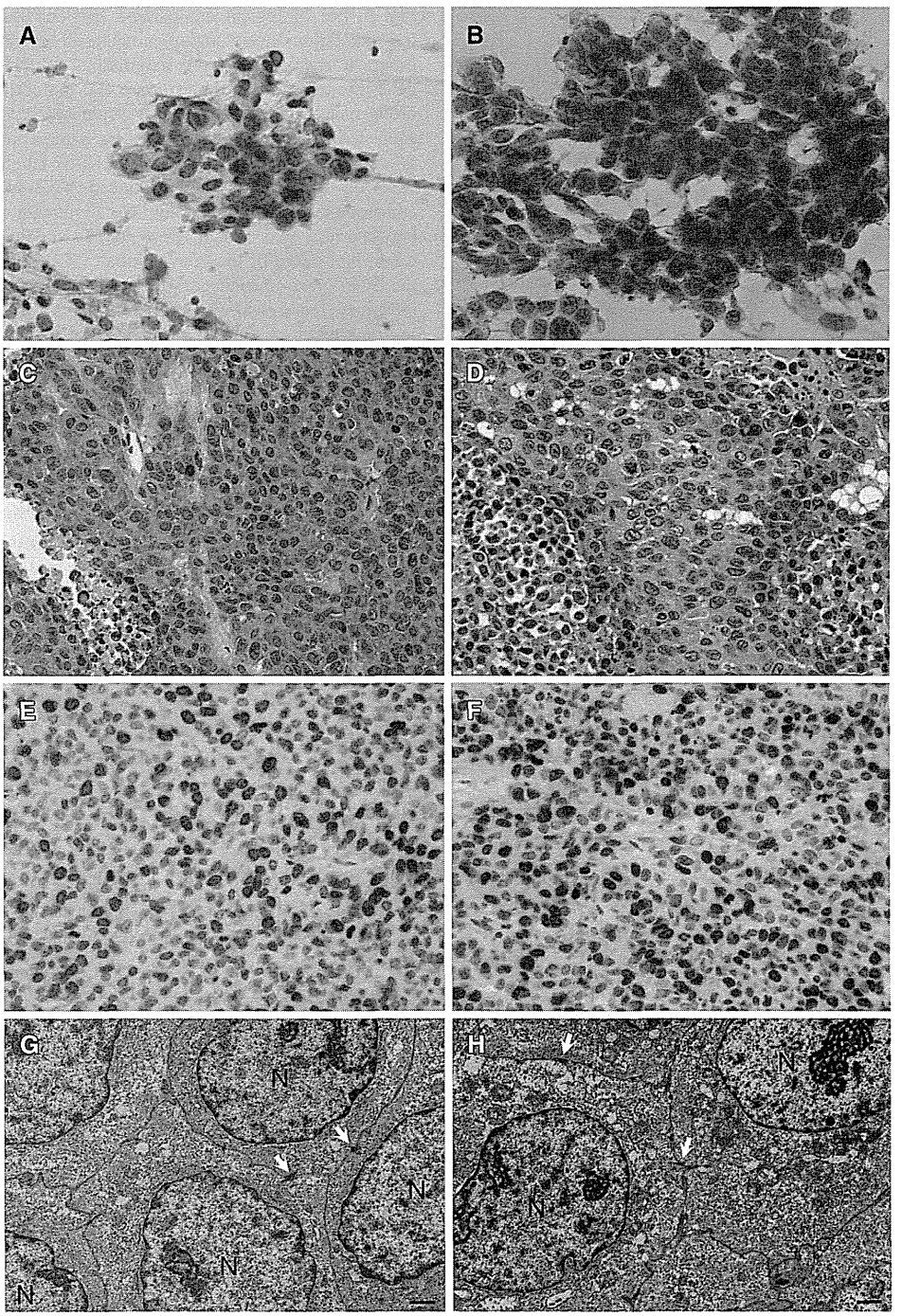

Fig. 4 Morphological comparison between conventional VX2 cells (**a**, **c**, **e**, **g**) and EGFP gene-introduced VX2 cells (**b**, **d**, **f**, **h**) that were transplanted and grown in rabbits. **a**, **b** Photomicrographs of scratch cytological samples. In both groups, the cancer cells demonstrate a feature of undifferentiated carcinoma with a moderate degree of pleomorphism and nuclear irregularity, a high nucleus-to-cytoplasm ratio, and enlarged nuclei with hyperchromatism. No cytological difference is evident between the two (Papanicolaou stain, objective 60×). **c**, **d** Photomicrographs of formalin-fixed, paraffin-embedded tissue samples. In both groups, lesions demonstrate the proliferation of undifferentiated atypical epithelial cells accompanied by mitotic figures and apoptotic bodies (hematoxylin and eosin stain, objective 40×). **e**, **f** Photomicrographs of cancer cells positive for Ki-67. No immunohistochemical difference is evident between the two (immunohistochemistry, objective 40×). **g**, **h** Transmission electron photomicrographs of cancer cells. In both groups, the cancer cells demonstrate a feature of undifferentiated carcinoma with moderate degree of pleomorphism and nuclear irregularity, a high nucleus-to-cytoplasm ratio, and enlarged nucleoli (N denotes nucleus), along with glycogen-rich cytoplasm with a small amount of intermediate filaments and endoplasmic reticulum with sparsely distributed desmosomes (*arrows*). No glandular structures are seen. No cytological difference is evident between the two (The *bar* indicates 1 μm)

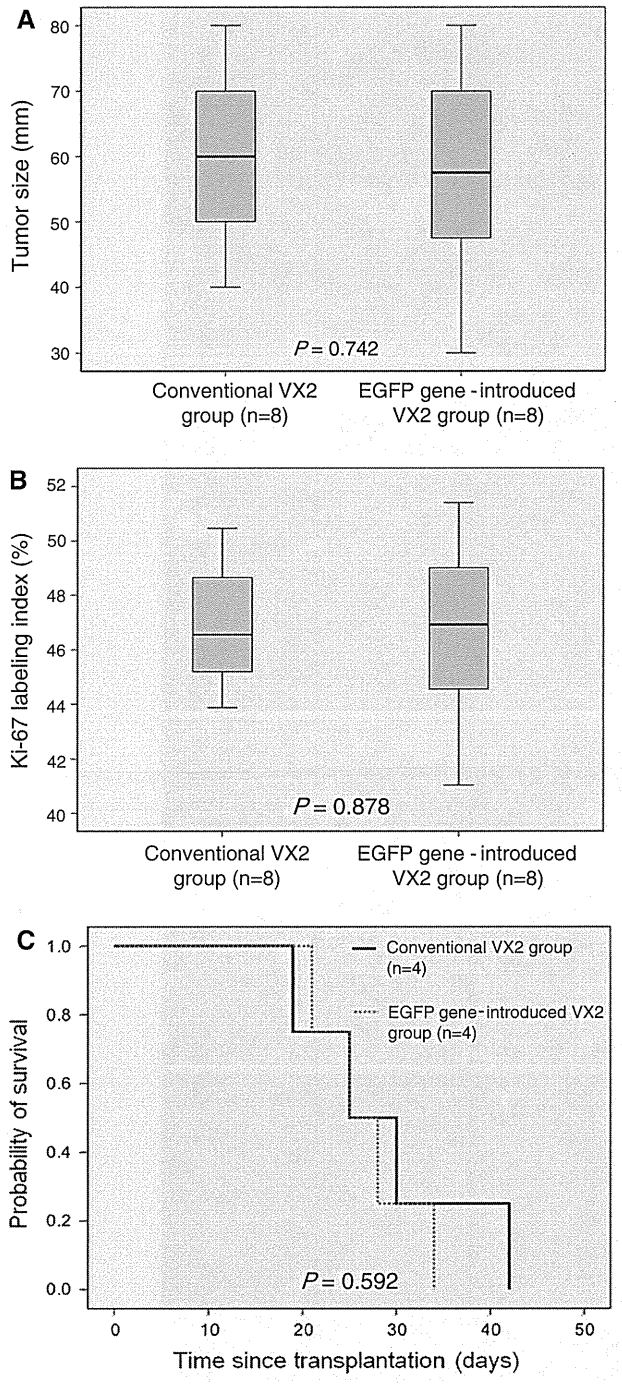

◀**Fig. 5** The biological comparison between the conventional VX2 transplantation group and the enhanced green fluorescent protein group. **a** Histogram of the longitudinal length (mm) of the EGFP gene-introduced VX2 rabbit group and the conventional VX2 rabbit group measured 3 weeks after transplantation. No significant difference was found between the two groups ($P = 0.742$, unpaired Student's t test). **b** Histogram of the Ki-67 labeling indices of cancer cells for the EGFP gene-introduced VX2 rabbit group and the conventional VX2 rabbit group. No significant difference was found between the two groups ($P = 0.878$, unpaired Student's t test). **c** Survival curve of the conventional VX2 rabbit group ($n = 4$) and the EGFP gene-introduced VX2 rabbit group ($n = 4$). No significant difference in survival was found between the two groups ($P = 0.592$, log-rank test)

paraffin-embedded tissue samples obtained from the conventional VX2 group, the positive rates in VX2 cancer cells for GFP, pan-cytokeratin and vimentin were 0 ± 0, 100.0 ± 0 % (mean ± SE) and 0.99 ± 0.60 % (mean ± SE; range 0.19–2.08), respectively; whereas fibroblasts, lymphocytes and endothelial cells in the conventional VX2 group were all positive for vimentin at 100 % level, and these stromal cells were entirely negative for GFP.

There were no significant differences with regard to morphology in scratch cytological samples, formalin-fixed, paraffin-embedded tissue samples, and electron microscopic samples between the EGFP gene-introduced VX2 tumors and the conventional VX2 tumors (Fig. 4a–h). In both groups, VX2 cancer cells were morphologically consistent with undifferentiated carcinoma; they were characterized by undifferentiated epithelial features with a moderate degree of pleomorphism and nuclear irregularity, a high nucleus-to-cytoplasm ratio, enlarged nuclei with hyperchromatism, and a large number of mitotic figures and apoptotic bodies, along with a varying degree of necrosis.

The longitudinal length of the tumors was 57.5 ± 5.8 mm (mean ± SE; range 30–80) in the EGFP gene-introduced VX2-transplanted rabbit group and 60.0 ± 4.6 mm (mean ± SE; range 40–80) in the conventional VX2-transplanted rabbit group. No significant difference was found in the longitudinal tumor size between the groups ($P = 0.742$, unpaired Student's t test; Fig. 5a).

The Ki-67 labeling indices of cancer cells in the hot spots were 46.7 ± 1.2 % (mean ± SE; range 41.0–51.4) in the EGFP gene-introduced VX2 rabbit group and 46.9 ± 0.8 % (mean ± SE; range 43.9–50.4) in the conventional VX2 rabbit group. Statistically, there was no significant difference in the Ki-67 labeling index between the two groups ($P = 0.878$, unpaired Student's t test; Fig. 5b).

Autopsy findings and survival analysis

Post-mortem pathological inspection confirmed that all VX2-transplanted rabbits died from cancer with multiple lung metastases. The survival analysis revealed that the median survival time of the conventional VX2 rabbit group and the EGFP gene-introduced VX2 rabbit group was 25 days (range of 21–34 and 21–42 days, respectively). No significant difference in survival was observed between the two groups ($P = 0.592$; Fig. 5c).

Discussion

In the present study, we could generate successively transplantable rabbit VX2 cancer cells that express EGFP. To our knowledge, this type of VX2 model has not been reported to date.

However, there are some weaknesses in the present study to emphasize this new model as a perfect one. First, we performed transplantation of EGFP gene-introduced VX2 cells using a small number of rabbits at the same time, so that biological heterogeneity in each rabbit is not precisely examined. Second, we performed successive transplantation only four times, so that it is unclear how many successions can be possible in this model. Although answering these questions is not within the scope of the present study, we think, in view of our primary findings that biological heterogeneity and successive transplantability in this model are largely as same as those in the conventional VX2 model.

One can assume a possibility that EGFP gene might have been unexpectedly introduced into stromal cells since there is a report describing that the primary cultures of rabbit VX2 cells are heterogeneous and contain at least two cell types that are different: epithelial cells (originating from cancer cells) and fibroblast-like cells (originating from the host's stroma) [17]. However, the possibility of such EGFP gene contamination is entirely refuted by our finding that green fluorescent protein expression was observed only in VX2 cancer cells and not in fibroblasts, lymphocytes and endothelial cells in histological samples. We therefore think that the very high specificity (100 %) and the high sensitivity (84.3 %) of EGFP expression make this new model useful for identifying VX2 cells in certain organs or locations where neoplastic cells morphologically mimic non-neoplastic cells and both cells share common markers. In addition, this EGFP-expressing VX2 transplantation model will enable the movement of cancer cells to be tracked, making this new model valuable in studies of cancer migration or metastasis in vivo. The methodology used in this study may be applied to the expression analysis of other specific proteins of interest that regulate tumor growth or metastasis in the VX2 cancer model.

The value and need of the cancer-bearing rabbit model should be discussed. The rabbit VX2 allograft model has long been utilized for studies of stromal responses, metastatic behaviors and therapeutic effects owing to their organ size and biological resemblance to human cancers [18–26]. However, they may represent only a part of the value of this model. Rabbits possess a lymphatic system closer to humans than mice or rats [27–42]. For this reason, we think that rabbits can be an attractive cancer-bearing model for studying in conjunction with the lymphatic system.

In conclusion, the major accomplishment of the present study is that VX2 cells can be genetically altered, visualized by EGFP, and successively transplanted without significant alteration of morphological and biological properties compared to those of the conventional model.

Acknowledgments This research was supported in part by Grants-in-Aid for Scientific Research from the Ministry of Education, Culture, Sports, Science and Technology of Japan (No. 20790993 and No. 24590242 to H. Oshiro, No. 24700501 to T. Nagai), Exploratory Research from the Yokohama Foundation for Advancement of Medical Science (to H. Oshiro), Medical Research from Tokyo Medical University Cancer Center (to H. Oshiro).

Conflict of interest We declare that we have no conflict of interest regarding this study.

References

1. Shiomi M (2009) Rabbit as a model for the study of human diseases. In: Houdebine L-M, Fan J (eds) Rabbit biotechnology. Springer Science, New York, pp 49–63
2. Shope RE, Hurst EW (1933) Infectious papillomatosis of rabbits with note on histopathology. J Exp Med 58:607–624
3. Rous P, Beard JW (1935) Progression to carcinoma of virus-induced rabbit papillomatosis. J Exp Med 62:523–548
4. Kidd JG, Rous P (1940) A transplantable rabbit carcinoma originating in a virus-induced papilloma and containing the virus in masked or altered form. J Exp Med 71:813–838
5. Rous P, Kidd JG, Smith WE (1952) Experiments on the cause of the rabbit carcinomas derived from virus-induced papillomas. II. Loss by the VX2 carcinoma of the power to immunize hosts against the papilloma virus. J Exp Med 96:159–174
6. Mei LJ, Yang XJ, Tang L, Hassan AH, Yonemura Y, Li Y (2010) Establishment and identification of a rabbit model of peritoneal carcinomatosis from gastric cancer. BMC Cancer 10:124
7. Chalfie M, Kine SR (2005) Methods of biochemical analysis, green fluorescent protein properties, applications and protocols, 2nd edn. Wiley, Hoboken, pp 1–488
8. Galasko CSB, Haynes DW (1976) Survival of VX2 carcinoma cells in vivo. Eur J Cancer 12:1025–1026
9. Shah SA, Dickson JA (1978) Preservation of enzymatically prepared rabbit VX2 tumour cells in vitro. Eur J Cancer 14:447–448
10. Georges E, Breitburd R, Jibard N, Orth G (1985) Two Shope papillomavirus-associated VX2 carcinoma cell lines with different levels of keratinocyte differentiation and transplantability. J Virol 55:246–250
11. Osato T, Ito Y (1967) In vitro cultivation and immunofluorescent studies of transplantable carcinomas VX2 and VX7. Persistence of a Shope virus-related antigenic substance in the cells of both tumors. J Exp Med 126:881–886
12. Dabbous MK, Roberts AN, Brinkley SB (1977) Collagenase and neutral protease activities in cultures of rabbit VX-2 carcinoma. Cancer Res 37:3537–3544
13. Dabbous MK, Sobhy C, Roberts AN, Brinkley B (1977) Changes in the collagenolytic activity released by primary VX-2 carcinoma cultures as a function of tumor growth. Mol Cell Biochem 16:37–42
14. Easty DM, Easty GC (1982) Establishment of an in vitro cell line from the rabbit VX2 carcinoma. Virchows Arch B Cell Pathol Incl Mol Patho 39:333–337

15. Handal JA, Schulz JF, Florez GB, Kwok SC, Khurana JS, Samuel SP (2013) Creation of rabbit bone and soft tissue tumor using cultured VX2 cells. J Surg Res 179:e127–e132
16. Proschek D, Tonak M, Kafchitsas K, Zangos S, Mack MG, Theisen A, Kurth AA (2011) Direct implantation of VX-2 carcinoma: a new rabbit bone model using a three-dimensional matrix as a carrier for the tumor cells. Eur Surg Res 47:154–158
17. Dabbous MK, El-Torky M, Haney L, Sobhy N, Brinkle SB (1983) Cytogenetic analysis of collagenase-releasing rabbit VX-2 carcinoma-derived cells. Exp Mol Pathol 38:1–21
18. Galasko CSB (1976) Mechanisms of bone destruction in the development of skeletal metastases. Nature 263:507–508
19. Galasko CSB, Bennett A (1976) Relationship of bone destruction in skeletal metastases to osteoclast activation and prostaglandins. Nature 263:508–510
20. Toole BP, Biswas C, Gross J (1979) Hyaluronate and invasiveness of the rabbit V2 carcinoma. Proc Natl Acad Sci USA 76:6299–6303
21. StrÃ¤uli P, In-Albon A, Haemmerli G (1983) Morphological studies on V2 carcinoma invasion and tumor-associated connective tissue changes in the rabbit mesentery. Cancer Res 43:5403–5410
22. Haemmerli G, MÃ¼ller-Glauser W, Bruckner P, Hauser-Urfer I, StrÃ¤uli P (1985) Tumor-associated desmoplasia in the rabbit mesentery characterized by morphological, biochemical and cytophotometric methods. Int J Cancer 35:527–534
23. Stewart EE, Sun H, Chen X, Schafer PH, Chen Y, Garcia BM, Lee TY (2012) Effect of an angiogenesis inhibitor on hepatic tumor perfusion and the implications for adjuvant cytotoxic therapy. Radiology 264:68–77
24. Tang L, Mei LJ, Yang XJ, Huang CQ, Zhou YF, Yonemura Y, Li Y (2011) Cytoreductive surgery plus hyperthermic intraperitoneal chemotherapy improves survival of gastric cancer with peritoneal carcinomatosis: evidence from an experimental study. J Transl Med 9:53
25. Yu H, Zhu GY, Xu RZ, Niu HZ, Lu Q, Li GZ, Wang ZY, Zhang DS, Gu N, Teng GJ (2011) Arterial embolization hyperthermia using As_2O_3 nanoparticles in VX2 carcinoma-induced liver tumors. PLoS One 6:e17926
26. Lee JY, Choi BI, Son KR, Lee JM, Kim SJ, Park HS, Chang JM, Choi SH, Kim MA, Moon WK (2012) Lymph node metastases from gastric cancer: gadofluorine M and gadopentetate dimeglumine MR imaging in a rabbit model. Radiology 263:391–400
27. Hayakawa T (1997) Comparative anatomy of the mammalian lymphatic system. In: Uchino S, Kato S, Ohtani O (eds) Lymphatics. Nishimura-shoten, Niigata, pp 286–295 (in Japanese)
28. Spira A (1962) The lymph node group (lymphocentra) in mammals: an attempt at homology. Anat Anz 111:294–364 (in German)
29. Kawashima Y, Sugimura M, Hwang Y-C, Kudo N (1964) The lymph system in mice. Jap J Vet Res 12:67–81
30. Seo S (1981) Anatomical study of the lymphatic system in rats. Tokyo Jikeikai Med J 96:642–662 (in Japanese with English abstract)
31. Nishida K (1954) About the lymphatic system in rabbits. Kumamoto Igakkai Zasshi 28:295–318 (in Japanese)
32. Kutsuna M (1966) Anatomical study of the lymphatic trunks in man and mammals. Kumamoto Med J 19:47–58
33. Kutsuna M (1968) Lymphatic trunks. In: Kutsuna M (ed) Anatomie des Lymphsystems der Japaner. Kanehara, Tokyo, pp 211–225 (in Japanese)
34. Hayakawa T, Koda M, Fukushima O, Kosugi K, Tokudome M, Yamashita H (1986) A comparative anatomical study of the lymphatic system of the lung in mammals: 6. Findings in rabbit. Jpn J Lymphol 9:63–68 (in Japanese with English abstract)
35. Murakami F (1967) Comparative anatomical study on the communication of the intrathoracic lymphatic system with the cervical lymphatic system. Kumamoto Igakkai Zasshi 41:267–306 (in Japanese)
36. Kutsuna M (1965) Intrathoracic lymph flow, with special regard to the communication of intrathoracic lymph vessels with cervical lymph nodes. Kumamoto Med J 18:228–233
37. Murakami G (2002) Last-intercalated node and direct lymphatic drainage into the thoracic duct from the thoracoabdominal viscera. Jpn J Thorac Cardiovasc Surg 50:93–103
38. Riquet M, Assouad J, Bagan P, Foucault C, Le Pimpec Barthes F, Dujon A, Danel C (2005) Skip mediastinal lymph node metastasis and lung cancer: a particular N2 subgroup with a better prognosis. Ann Thorac Surg 79:225–233
39. Sakao Y, Miyamoto H, Yamazaki A, Ou S, Shiomi K, Sonobe S, Sakuraba M (2006) The spread of metastatic lymph nodes to the mediastinum from left upper lobe cancer: results of superior mediastinal nodal dissection through a median sternotomy. Eur J Cardiothorac Surg 30:543–547
40. Sakao Y, Miyamoto H, Oh S, Takahashi N, Sakuraba M (2007) Clinicopathological factors associated with unexpected N3 in patients with mediastinal lymph node involvement. J Thorac Oncol 2:1107–1111
41. Anami K, Yamashita S, Yamamoto S, Chujo M, Tokuishi K, Moroga T, Mori H, Kawahara K (2013) Contralateral mediastinal lymph node micrometastases assessed by video-assisted thoracoscopic surgery in stage I non-small cell left lung cancer. Eur J Cardiothorac Surg 43:778–782
42. Feng ZX, Zhao LJ, Guan Y, Sun Y, Meng MB, Ji K, Wang P (2013) Identification of risk factors and characteristics of supraclavicular lymph node metastasis in patients with small cell lung cancer. Med Oncol 30:493

J Physiol Sci (2015) 65:195–200
DOI 10.1007/s12576-014-0354-3

SHORT COMMUNICATION

Oscillation of cAMP and Ca^{2+} in cardiac myocytes: a systems biology approach

Takehisa Kamide · Satoshi Okumura · Samik Ghosh · Yoko Shinoda · Yasumasa Mototani · Yoshiki Ohnuki · Huiling Jin · Wenqian Cai · Kenji Suita · Itaru Sato · Masanari Umemura · Takayuki Fujita · Utako Yokoyama · Motohiko Sato · Kazuharu Furutani · Hiroaki Kitano · Yoshihiro Ishikawa

Received: 25 September 2014 / Accepted: 18 December 2014 / Published online: 14 January 2015

Abstract Cyclic adenosine monophosphate (cAMP) and Ca^{2+} levels may oscillate in harmony within excitable cells; a mathematical oscillation loop model, the Cooper model, of these oscillations was developed two decades ago. However, in that model all adenylyl cyclase (AC) isoforms were assumed to be inhibited by Ca^{2+}, and it is now known that the heart expresses multiple AC isoforms, among which the type 5/6 isoforms are Ca^{2+}-inhibitable whereas the other five (AC2, 3, 4, 7, and 9) are not. We used a computational systems biology approach with CellDesigner simulation software to develop a comprehensive graphical map and oscillation loop model for cAMP and Ca^{2+}. This model indicated that Ca^{2+}-mediated inhibition of AC is essential to create oscillations of Ca^{2+} and cAMP, and the oscillations were not altered by incorporation of phosphodiesterase-mediated cAMP hydrolysis or PKA-mediated inhibition of AC into the model. More importantly, they were created but faded out immediately in the co-presence of Ca^{2+}-noninhibitable AC isoforms. Because the subcellular locations of AC isoforms are different, spontaneous cAMP and Ca^{2+} oscillations may occur within microdomains containing only Ca^{2+}-inhibitable isoforms in cardiac myocytes, which might be necessary for fine tuning of excitation–contraction coupling.

Keywords Adenlyl cyclase · Subtype · Computational analysis · Oscillation · Cyclic AMP · Calcium

Electronic supplementary material The online version of this article (doi:10.1007/s12576-014-0354-3) contains supplementary material, which is available to authorized users.

T. Kamide · S. Okumura · H. Jin · W. Cai · K. Suita · I. Sato · M. Umemura · T. Fujita · U. Yokoyama · M. Sato · Y. Ishikawa (✉)
Cardiovascular Research Institute, Yokohama City University Graduate School of Medicine, 3-9 Fukuura, Kanazawa-ku, Yokohama 236-0004, Japan
e-mail: yishikaw@yokohama-cu.ac.jp

S. Okumura (✉) · Y. Shinoda · Y. Mototani · Y. Ohnuki
Department of Physiology, Tsurumi University School of Dental Medicine, 2-1-2 Tsurumi, Tsurumi-ku, Yokohama 230-8501, Japan
e-mail: okumura-s@tsuruni-u.ac.jp

S. Ghosh · H. Kitano
The Systems Biology Institute, Minato, Tokyo 108-0071, Japan

M. Sato
Department of Physiology, Aichi Medical University, Nagakute, Aichi 480-1195, Japan

K. Furutani
Department of Pharmacology, Graduate School of Medicine, Osaka University, Osaka 565-0871, Japan

K. Furutani
Center for Advanced Medical Engineering and Informatics, Osaka University, Osaka 565-0871, Japan

H. Kitano
Okinawa Institute of Science and Technology Graduate School, Onna-Son, Okinawa 904-0412, Japan

H. Kitano
Laboratory for Disease Systems Modeling, Riken Center for Integrative Medical Sciences, Yokohama 230-0045, Japan

Introduction

β-Adrenergic receptor (β-AR) signaling is of crucial importance in regulating normal cardiac function, and abnormality of β-AR signaling contributes to the development of heart failure via altered cyclic AMP (cAMP) and calcium (Ca^{2+}) signaling [1–3]. Cardiac excitation–contraction coupling (E–C coupling) is the process that links electrical excitation of cardiac myocytes to contraction of heart muscle. Ca^{2+} is essential for cardiac electrical activity and is a direct activator of myofilaments, causing both contraction and relaxation [4–6]. Dysregulation of cAMP and the subsequent Ca^{2+} oscillation are fundamental causes of both contractile and diastolic dysfunction, and arrhythmia among heart failure patients [1, 3, 5, 7–10].

Adenylyl cyclase (AC) is a membrane-bound enzyme that catalyzes the conversion of ATP to cAMP [1, 11]. cAMP, an intracellular second messenger, activates protein kinase A (PKA), leading to phosphorylation of multiple molecules involved in cardiac contraction, including the L-type Ca^{2+}-channel [1]. Phosphorylation of the L-type Ca^{2+}-channel is known to increase the influx of Ca^{2+}, resulting in increased intracellular levels of Ca^{2+}. In the 1990s, AC isoforms directly inhibited by Ca^{2+} were identified, i.e., types 5 and 6 AC isoforms (AC5 and AC6) [11–14]. Because these isoforms are dominantly expressed in the heart, it was proposed that cAMP levels may oscillate in harmony with Ca^{2+} levels; an increase in cAMP, as generated by AC5/6, phosphorylates L-type Ca^{2+} channels, and induces influx of Ca^{2+} into the cytosol [11]. An increase of cytosolic Ca^{2+} inhibits AC5/6 and reduces phosphorylation of the L-type Ca^{2+} channel. Thus, the activity of AC5/6 and the L-type Ca^{2+} channel may work synergistically to generate an oscillation loop of cAMP and Ca^{2+} in cardiac myocytes [11].

It is now well known that the heart expresses not only AC5 and AC6, but also many other AC isoforms (AC2, 3, 4, 5, 6, 7, and 9) [2]. Although these isoforms are all expressed in the heart, recent studies have indicated they may have different subcellular locations [15, 16]. AC5 is a major cardiac isoform in adults, and AC6 is a fetal or neonatal cardiac AC isoform [1, 17–19]. AC5 and AC6 share most, if not all, of their biochemical properties, and are inhibited not only by Ca^{2+}, but also by Gi and PKA [2, 11, 13, 20–22]. In contrast, the other AC isoforms (AC2, 3, 4, 7, and 9), which are ubiquitously expressed throughout the body, are not inhibited by Ca^{2+}, Gi, or PKA [13], and their involvement in cAMP and Ca^{2+} oscillations is poorly understood.

We therefore examined the involvement of AC isoforms in cAMP and Ca^{2+} oscillations [1, 12]. Because it is difficult to examine these issues by means of traditional in vitro or in vivo biochemical approaches, we used a computational systems biology approach with CellDesigner software, a recently developed, structure diagram editor for drawing gene-regulatory and biochemical networks [23–25].

Materials and methods

CellDesigner version 4.2 (http://www.celldesigner.org/) enables users to describe molecular interactions by using well-defined and consistent graphical notions and to create a comprehensive model incorporating positive feedforward or negative feedback loops among AC, cAMP, Ca^{2+}, phosphodiesterase (PDE), and PKA within the β-AR signaling pathway [23–25].

The CellDesigner notation used in this paper is briefly illustrated for a simple reaction scheme in Supplemental Fig. 1. Protein A is transformed to protein B and protein C promotes this transition (Supplemental Fig. 1a). Supplemental Fig. 1b shows the notation for degradation (upper) or production (lower) of protein A; their balance determines the concentration of protein A in cells under physiological conditions.

In this study, most of the variables were the same as in Cooper's original model [12]; in future work, it would be desirable to optimize the variables used in the oscillation loop model to match physiological conditions.

The formulas and values used to generate the oscillation models shown in the figures can be found in the online Supplemental methods and Supplemental Tables 1–3, available on http://www.link.springer.com/journal/12576.

Results

Cooper's model mimicked by CellDesigner

We first mimicked Cooper's original model by using CellDesigner to create a graphical comprehensive map (Fig. 1a) and oscillation loop model of cAMP and Ca^{2+} (Fig. 1b). We also incorporated the activity of PKA and AC. For AC, we used AC5/6 because they are the major cardiac isoforms and are directly inhibited by Ca^{2+} [2, 13]. We obtained stable and spontaneous oscillation curves for cAMP and Ca^{2+}, as demonstrated in the original model [12]. The activity of AC and PKA also oscillated (Fig. 1b).

The formulas and values used to generate this oscillation model are shown in online Supplemental methods and Supplemental Table 1.

Incorporation of the PDE-mediated cAMP hydrolysis

Intracellular cAMP concentration is determined by the balance between its production via AC and its hydrolysis

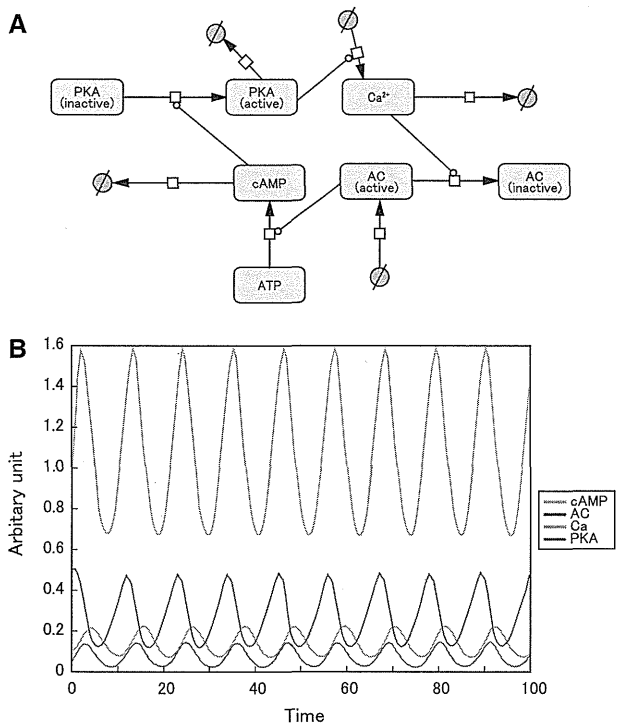

Fig. 1 Cooper's model mimicked by CellDesigner. **a** Graphical notations used in CellDesigner to depict Cooper's model. **b** Computational oscillation loop of β-AR signaling molecules. cAMP, Ca^{2+}, AC, and PKA formed a stable and persistent negative feedback loop. The intracellular concentration of cAMP at baseline (0 min) was taken as 1 (arbitrary units)

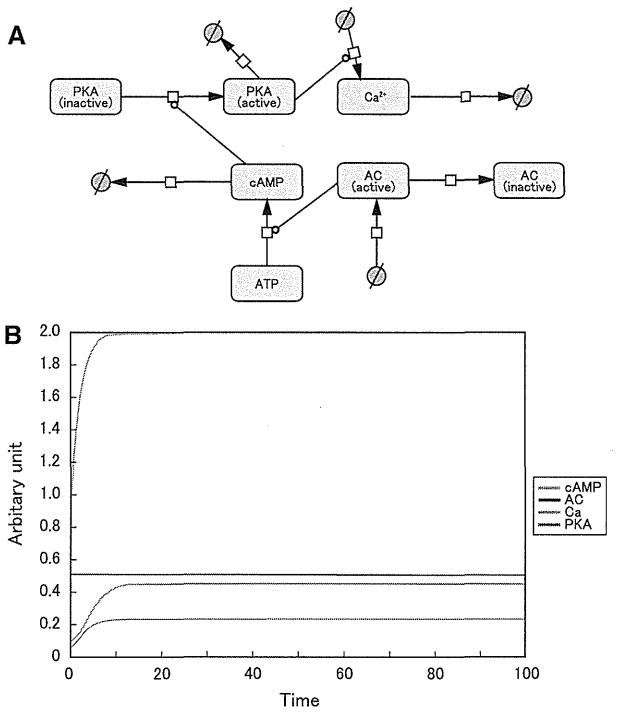

Fig. 2 Effects of Ca^{2+}-mediated inhibition of AC. **a** Graphical notation used in CellDesigner to depict β-AR signaling molecules AC, cAMP, Ca^{2+}, and PKA. Ca^{2+}-mediated inhibition of AC was deleted from Cooper's original model. **b** Computational oscillation loop of β-AR signaling molecules. cAMP, Ca^{2+}, AC, and PKA did not form a negative feedback loop. The intracellular concentration of cAMP at baseline (0 min) was taken as 1 (arbitrary units)

via PDE in the heart under physiological and pathological conditions [26]. Because PDE is activated by cAMP, we incorporated its activity into the model (Supplemental Fig. 2a). We found that oscillations of the molecules involved in the β-AR signaling pathway were maintained, even though their amplitudes were increased by approximately 1.6-fold, compared with those of Cooper's original model (Supplemental Fig. 2b). Thus, PDE-mediated cAMP hydrolysis did not appear to change the behavior of the oscillation, but exaggerated its amplitude.

The formulas and values used to generate this oscillation model are shown in online Supplemental methods and Supplemental Table 2.

Effect of Ca^{2+}-mediated inhibition of AC

The heart expresses multiple AC isoforms (AC2, 3, 4, 5, 6, 7, and 9) [2], of which AC5 and AC6 are directly inhibited by submicromolar Ca^{2+} [2, 13]. Thus, to examine the effect of Ca^{2+}-mediated inhibition of AC, we modeled the situation in which all AC isoforms in the heart are not Ca^{2+}-inhibitable in the heart (Fig. 2a). As shown in Fig. 2b, we found that no oscillation appeared. This result indicates that the presence of Ca^{2+}-inhibitable AC isoforms is essential for stable and spontaneous cAMP and Ca^{2+} oscillations to occur.

The formulas and values used to generate this oscillation model are shown in online supplemental methods and supplemental Table 1.

Incorporation of PKA-mediated inhibition of cardiac AC isoforms into the model

Recent studies have indicated that AC5 and AC6 are inhibited not only by Ca^{2+}, but also by PKA [13, 20–22]. Therefore, we next incorporated PKA-mediated inhibition into Cooper's model (Fig. 3a). Oscillations of cAMP and Ca^{2+}, as well as AC and PKA, were observed, but the amplitudes were reduced by approximately 13 %, compared with those in Cooper's original model (Fig. 3b). Thus, PKA-mediated inhibition of cardiac AC isoforms did not seem to change the behavior of the oscillation, but reduced its amplitude.

The formulas and values used to generate this oscillation model are shown in online Supplemental methods and Supplemental Table 1.

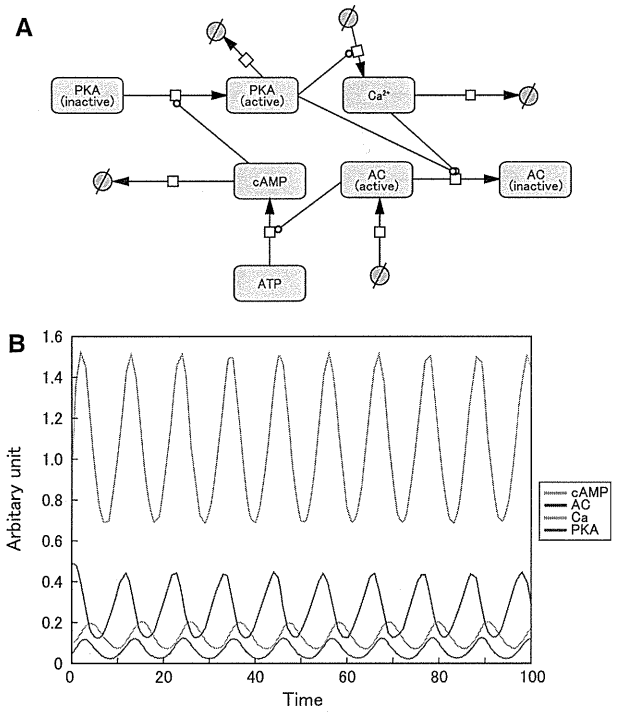

Fig. 3 Effects of PKA-mediated inhibition of AC. **a** Graphical notation used in CellDesigner to depict β-AR signaling molecules AC, cAMP, Ca^{2+}, and PKA. PKA-mediated inhibition of AC was incorporated into Cooper's original model. **b** Computational oscillation loop of β-AR signaling molecules. cAMP, Ca^{2+}, AC, and PKA formed a stable and spontaneous negative feedback loop. The intracellular concentration of cAMP at baseline (0 min) was taken as 1 (arbitrary units)

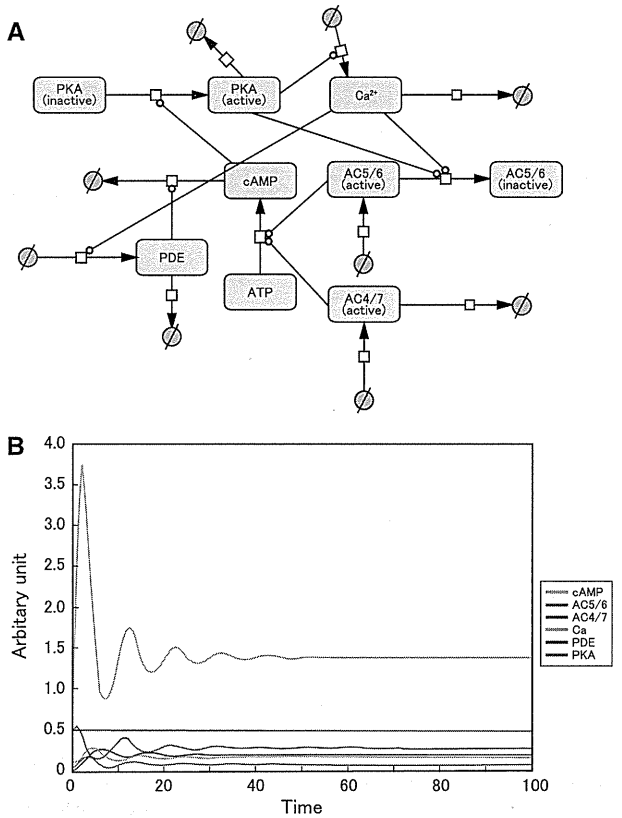

Fig. 4 Incorporation of Ca^{2+}-mediated inhibition of type 5/6 AC into the model. **a** Graphical notation used by CellDesigner to depict β-AR signaling molecules: cardiac AC subtypes (AC5/6), non-cardiac AC subtypes (AC4/7), cAMP, Ca^{2+}, and PKA. A negative feedback loop was not observed. **b** Computational oscillation loop of β-AR signaling molecules: cAMP, Ca^{2+}, AC5/6, PDE, and PKA did not form a continuous negative feedback loop, and then faded. However, essentially no oscillation occurred. The intracellular concentration of cAMP at baseline (0 min) was taken as 1 (arbitrary units)

Incorporation of Ca^{2+}-mediated inhibition of type 5/6 AC isoforms into the model

We then examined the model incorporating both Ca^{2+}-inhibitable (AC5/6) and non-inhibitable AC isoforms (AC2, 3, 4, 7, and 9) (Fig. 4a). Studies with transgenic mouse models in vivo have demonstrated that AC2, 3, 4, 7, and 9 contribute significantly to the total AC activity in the heart [2, 27], but, unlike AC5/6, are not subjected to PKA-mediated inhibition [13]. Oscillations of cAMP, Ca^{2+}, PKA, PDE, and AC5/6 were observed, and then faded. However, essentially, no oscillation of AC4/7 occurred (Fig. 4b). Thus, when both Ca^{2+}-inhibitable and Ca^{2+}-non-inhibitable AC isoforms coexist, continuous oscillation is not usually observed for cellular cAMP and Ca^{2+}.

The formulas and values used to generate this oscillation model are shown in online Supplemental methods and Supplemental Table 3.

Discussion

Control systems in vivo are dynamic and complex, and it is very difficult to predict systems behavior on the basis of biochemical studies of individual molecules. However, use of systems biology tools, for example CellDesigner, makes it feasible to simulate complex biochemical networks flexibly [28–30]. In this study, this software enabled us to study Ca^{2+} and cAMP oscillations under different conditions, e.g., in the presence or absence of Ca^{2+}-inhibitable and Ca^{2+}-non-inhibitable AC isoforms and other regulatory molecules, in silico, without the need for experimental assays [25].

First, we confirmed that the original oscillation model of cAMP and Ca^{2+} developed by Cooper in 1995 [12] can be effectively simulated by use of CellDesigner [23–25]. When the signaling pathway contained only Ca^{2+}-inhibitable AC isoforms (AC5/6), we found that stable and spontaneous oscillations occurred.

Inclusion of PDE-mediated cAMP hydrolysis or PKA-mediated inhibition of AC5/6 into Cooper's model did not seem to change the oscillation behavior, but altered the amplitude to a greater or lesser extent [13, 20–22, 26].

Inclusion of PKA-mediated inhibition of AC5/6 induced a decrease of the amplitude by approximately 13 % (Fig. 3), whereas inclusion of PDE-mediated cAMP hydrolysis increased the amplitude by approximately 1.6-fold (Supplemental Fig. 2), compared with those of Cooper's original model (Fig. 1).

Phosphorylation of the L-type Ca^{2+}-channel increases the Ca^{2+} concentration, and might form an ascending loop. In turn, cardiac AC isoforms (AC5/6) are inhibited by Ca^{2+} and this might form a descending loop. Importantly, AC5/6 are inhibited by PKA, which might reduce the amplitude of the oscillation loop [13, 22]. Conversely, PDE, in association with Ca^{2+}-mediated inhibition, forms the descending phase of cAMP and Ca^{2+} oscillation in cardiac myocytes [31, 32]. These data, together with our current findings, indicate that PKA may have both positive and negative regulatory effects on the amplitude of the cAMP and Ca^{2+} oscillation loop, whereas PDE may have a positive regulatory effect on the amplitude [31, 32].

In contrast, when AC isoforms were not Ca^{2+}-inhibitable, no oscillation occurred. Interestingly, when both Ca^{2+}-non-inhibitable and Ca^{2+}-inhibitable AC isoforms were included in the model, oscillation occurred, but decayed very rapidly. Inclusion of PDE-mediated cAMP hydrolysis did not change this behavior. Therefore, our simulations indicate that for stable and spontaneous oscillation, the presence of Ca^{2+}-inhibitable AC isoforms and the absence of Ca^{2+}-non-inhibitable AC isoforms are both required.

Further studies will be required to incorporate the effects of newly identified AC5/6-associated proteins, including Snapin, a SNAP25-binding protein, and PAM, a protein associated with Myc, on the cAMP and Ca^{2+} oscillations, because the findings of this study show that Ca^{2+}-inhibitable AC isoforms (AC5/6) are essential for the oscillations of cAMP and Ca^{2+} [2, 13, 15].

Because the heart expresses seven AC isoforms [1, 7], including both Ca^{2+}-inhibitable and Ca^{2+}-non-inhibitable isoforms, continuous cAMP and Ca^{2+} oscillation in cardiac myocytes may not always occur, on the basis of the above findings (Fig. 4). Studies using AC5-deficient mice from our laboratory have shown that nearly half of the AC activity within the heart may be because of Ca^{2+}-non-inhibitable AC isoforms [1, 2, 7, 9, 33, 34]. However, microenvironments in which only Ca^{2+}-inhibitable AC5/6 are accumulated, such as lipid rafts or caveolae, are believed to exist [15, 16]. Indeed, it has been reported that Ca^{2+}-sensitive AC isoforms (AC1, 5, 6, and 8) and their associated proteins, such as PKA, A-kinase anchoring proteins (AKAPs), anchored PDEs, non-anchored PDE, and transient receptor potential (TRP) 1/3, are present in lipid rafts in many cell types, including cardiac myocytes, whereas the Ca^{2+}-insensitive AC 2, 4, and 7 are excluded from the rafts [15]. Because intracellular cAMP and Ca^{2+} mediate a diverse array of cellular functions, oscillation of cAMP and Ca^{2+} concentration might be involved in receptor-mediated signal transduction, not only in excitable cells, for example cardiac myocytes, but also in non-excitable cells [35]. Further, the occurrence or disturbance of cAMP and Ca^{2+} oscillations might contribute to the development of cardiac dysfunction or arrhythmia.

Acknowledgments This study was supported in part by grants from the Ministry of Health, Labor, and Welfare (Dr Ishikawa), a Grant-in-Aid for Scientific Research on Innovative Areas (22136009), and Grants from the Japanese Ministry of Education, Culture, Sports, Science, and Technology (Drs Ishikawa, Okumura, Fujita, Sato, Yokoyama, Mototani), the National Cerebral and Cardiovascular Center (Dr Ishikawa), the Takeda Science Foundation (Dr Okumura), the Yokohama Foundation for Advancement of Medical Science (Dr Okumura), the Yokohama Academic Foundation (Dr Ohnuki), the Research Foundation for Community Medicine (Dr Okumura), and the Suzuken Memorial Foundation (Dr Okumura).

Conflict of interest The authors declare no potential conflicts of interest.

References

1. Okumura S, Suzuki S, Ishikawa Y (2009) New aspects for the treatment of cardiac diseases based on the diversity of functional controls on cardiac muscles: effects of targeted disruption of the type 5 adenylyl cyclase gene. J Pharmacol Sci 109:354–359
2. Okumura S, Kawabe J, Yatani A, Takagi G, Lee MC, Hong C, Liu J, Takagi I, Sadoshima J, Vatner DE, Vatner SF, Ishikawa Y (2003) Type 5 adenylyl cyclase disruption alters not only sympathetic but also parasympathetic and calcium-mediated cardiac regulation. Circ Res 93:364–371
3. Okumura S, Fujita T, Cai W, Jin M, Namekata I, Mototani Y, Jin H, Ohnuki Y, Tsuneoka Y, Bai Y, Suzuki S, Hidaka Y, Umemura M, Ichikawa Y, Yokoyama U, Sato M, Ishikawa F, Izumi-Nakaseko H, Adachi-Akahane S, Tanaka H, Ishikawa Y (2014) *EPAC1*-dependent phospholamban phosphorylation mediates the cardiac response to stresses. J Clin Invest 124:2785–2801
4. Ohnuki Y, Nishimura S, Sugiura S, Saeki Y (2008) Phosphorylation status of regulatory proteins and functional characteristics in myocardium of dilated cardiomyopathy of Syrian hamsters. J Physiol Sci 58:15–20
5. Bers DM (2002) Calcium and cardiac rhythms: physiological and pathophysiological. Circ Res 90:14–17
6. Ohnuki Y, Yamada T, Mototani Y, Umeki D, Shiozawa K, Fujita T, Saeki Y, Okumura S (2013) Effects of protein kinase a on the phosphorylation status and transverse stiffness of cardiac myofibrils. J Pharmacol Sci 123:279–283
7. Okumura S, Takagi G, Kawabe J, Yang G, Lee MC, Hong C, Liu J, Vatner DE, Sadoshima J, Vatner SF, Ishikawa Y (2003) Disruption of type 5 adenylyl cyclase gene preserves cardiac function against pressure overload. Proc Natl Acad Sci USA 100:9986–9990
8. Marks AR (2013) Calcium cycling proteins and heart failure: mechanisms and therapeutics. J Clin Invest 123:46–52
9. Okumura S, Vatner DE, Kurotani R, Bai Y, Gao S, Yuan Z, Iwatsubo K, Ulucan C, Kawabe J, Gjosh K, Vatner SF, Ishikawa Y (2007) Disruption of type 5 adenylyl cyclase enhances desensitization of cyclic adenosine monophosphate signal and

increases Akt signal with chronic catecholamine stress. Circulation 116:1776–1783
10. Ohnuki Y, Umeki D, Mototani Y, Jin H, Cai W, Shiozawa K, Suita K, Saeki Y, Fujita T, Ishikawa Y, Okumura S (2014) Role of cyclic AMP sensor epac1 in masseter muscle hypertrophy and myosin heavy chain transition induced by β_2-adrenoceptor stimulation. J Physiol 592:5461–5475
11. Ishikawa Y, Homcy CJ (1997) The adenylyl cyclases as integrators of transmembrane signal transduction. Circ Res 80:297–304
12. Cooper DM, Mons N, Karpen JW (1995) Adenylyl cyclases and the interaction between calcium and cAMP signalling. Nature 374:421–424
13. Hanoune J, Defer N (2001) Regulation and role of adenylyl cyclase isoforms. Annu Rev Pharmacol Toxicol 41:145–174
14. Katsushika S, Chen L, Kawabe J, Nilakantan R, Halnon NJ, Homcy C, Ishikawa Y (1992) Cloning and characterization of a sixth adenylyl cyclase isoform: types V and VI constitute a subgroup within the mammalian adenylyl cyclase family. Proc Natl Acad Sci USA 89:8774–8778
15. Willoughby D, Cooper DM (2007) Organization and Ca^{2+} regulation of adenylyl cyclases in cAMP microdomains. Physiol Rev 87:965–1010
16. Timofeyev V, Myers RE, Kim HJ, Woltz RL, Sirish P, Heiserman JP, Li N, Singapuri A, Tang T, Yarov-Yarovoy V, Yamoah EN, Hammond HK, Chiamvimonvat N (2013) Adenylyl cyclase subtype-specific compartmentalization: differential regulation of L-type Ca^{2+} current in ventricular myocytes. Circ Res 112:1567–1576
17. Ishikawa Y, Katsushika S, Chen L, Halnon NJ, Kawabe J, Homcy CJ (1992) Isolation and characterization of a novel cardiac adenylylcyclase cDNA. J Biol Chem 267:13553–13557
18. Espinasse I, Iourgenko V, Defer N, Samson F, Hanoune J, Mercadier JJ (1995) Type V, but not type VI, adenylyl cyclase mRNA accumulates in the rat heart during ontogenic development. Correlation with increased global adenylyl cyclase activity. J Mol Cell Cardiol 27:1789–1795
19. Tobise K, Ishikawa Y, Holmer SR, Im MJ, Newell JB, Yoshie H, Fujita M, Susannie EE, Homcy CJ (1994) Changes in type VI adenylyl cyclase isoform expression correlate with a decreased capacity for cAMP generation in the aging ventricle. Circ Res 74:596–603
20. Premont RT, Jacobowitz O, Iyengar R (1992) Lowered responsiveness of the catalyst of adenylyl cyclase to stimulation by GS in heterologous desensitization: a role for adenosine 3′,5′-monophosphate-dependent phosphorylation. Endocrinology 131:2774–2784
21. Chen Y, Harry A, Li J, Smit MJ, Bai X, Magnusson R, Pieroni JP, Weng G, Iyengar R (1997) Adenylyl cyclase 6 is selectively regulated by protein kinase A phosphorylation in a region involved in Galphas stimulation. Proc Natl Acad Sci USA 94:14100–14104
22. Iwami G, Kawabe J, Ebina T, Cannon PJ, Homcy CJ (1995) Regulation of adenylyl cyclase by protein kinase A. J Biol Chem 270:12481–12484
23. Kitano H, Funahashi A, Matsuoka Y, Oda K (2005) Using process diagrams for the graphical representation of biological networks. Nat Biotechnol 23:961–966
24. Funahashi A, Jouraku A, Matsuoka Y, Kitano H (2007) Integration of Cell Designer and SABIO-RK. In Silico Biol 7:S81–S90
25. Matsuoka Y, Funahashi A, Ghosh S, Kitano H (2014) Modeling and simulation using Cell Designer. Methods Mol Biol 1164: 121–145
26. Sato N, Asai K, Okumura S, Takagi G, Shannon RP, Fujita-Yamaguchi Y, Ishikawa Y, Vatner SF, Vatner DE et al (1999) Mechanisms of desensitization to a PDE inhibitor (milrinone) in conscious dogs with heart failure. Am J Physiol 276:H1699–H1705
27. Tang T, Gao MH, Lai NC, Firth AL, Takahashi T et al (2008) Adenylyl cyclase type 6 deletion decreases left ventricular function via impaired calcium handling. Circulation 117:61–69
28. Autiero I, Costantini S, Colonna G (2009) Modeling of the bacterial mechanism of methicillin-resistance by a systems biology approach. PLoS One 4:e6226
29. Grieco L, Calzone L, Bernard-Pierrot I, Radvanyi F, Kahn-Perles B, Thieffy D (2013) Integrative modelling of the influence of MAPK network on cancer cell fate decision. PLoS Comput Biol 9:e1003286
30. Wu G, Zhu L, Dent JE, Nardini C (2010) A comprehensive molecular interaction map for rheumatoid arthritis. PLoS One 5:e10137
31. Mika D, Richter W, Westenbroek RE, Catterall WA, Conti M (2014) PDE4B mediates local feedback regulation of β_1-adrenergic cAMP signaling in a sarcolemmal compartment of cardiac myocytes. J Cell Sci 127:1033–1042
32. Masaki N, Fujimoto K, Honda-Kitahara M, Hada E, Sawai S (2013) Robustness of self-organizing chemoattractant field arising from precise pulse induction of its breakdown enzyme: a single-cell level analysis of PDE expression in Dictyostelium. Biophys J 104:1191–1202
33. Okumura S, Tsunematsu T, Bai Y, Jiao Q, Ono S, Suzuki S, Kurotani R, Sato M, Minamisawa S, Umemura S, Ishikawa Y (2008) Type 5 adenylyl cyclase plays a major role in stabilizing heart rate in response to microgravity induced by parabolic flight. J Appl Physiol 1985 105:173–179
34. Bai Y, Tsunematsu T, Jiao Q, Ohnuki Y, Mototani Y, Shiozawa K, Jin M, Cai W, Jin HL, Fujita T, Ichikawa Y, Suita K, Kurotani R, Yokoyama U, Sato M, Iwatsubo K, Isikawa Y (2012) Pharmacological stimulation of type 5 adenylyl cyclase stabilizes heart rate under both microgravity and hypergravity induced by parabolic flight. J Pharmacol Sci 119:381–389
35. Dolmetsch RE, Xu K, Lewis RS (1998) Calcium oscillations increase the efficiency and specificity of gene expression. Nature 392:933–936

Biochemical and Biophysical Research Communications xxx (2015) 1–5

Contents lists available at ScienceDirect

Biochemical and Biophysical Research Communications

journal homepage: www.elsevier.com/locate/ybbrc

Coupling of β_1-adrenergic receptor to type 5 adenylyl cyclase and its physiological relevance in cardiac myocytes

Takashi Tsunematsu [a], Satoshi Okumura [a, b, *], Yasumasa Mototani [b], Yoshiki Ohnuki [b], Huiling Jin [a], Wenqian Cai [a], Kenji Suita [a], Itaru Sato [a], Masanari Umemura [a], Utako Yokoyama [a], Motohiko Sato [a, c], Takayuki Fujita [a], Yoshihiro Ishikawa [a, **]

[a] Cardiovascular Research Institute, Yokohama City University Graduate School of Medicine, Yokohama 236-0004, Japan
[b] Department of Physiology, Tsurumi University School of Dental Medicine, Yokohama 230-8501, Japan
[c] Department of Physiology, Aichi Medical University, Nagakute, Aichi 480-1195, Japan

ARTICLE INFO

Article history:
Received 27 December 2014
Available online xxx

Keywords:
β-receptor
Adenylyl cyclase
Heart
Cyclic AMP
Apoptosis

ABSTRACT

Myocardial β-adrenergic receptor (β-AR) β_1- and β_2-subtypes are highly homologous, but play opposite roles in cardiac apoptosis and heart failure, as do cardiac adenylyl cyclase (AC) subtypes 5 (AC5) and 6 (AC6): β_1-AR and AC5 promote cardiac remodeling, while β_2-AR and AC6 activate cell survival pathways. However, the mechanisms involved remain poorly understood. We hypothesized that AC5 is coupled preferentially to β_1-AR rather than β_2-AR, and we examined this idea by means of pharmacological and genetic approaches. We found that selective inhibition of AC5 with 2′5′-dideoxyadenosine significantly suppressed cAMP accumulation and cardiac apoptosis induced by selective β_1-AR stimulation, but had no effect on cAMP accumulation and cardiac apoptosis in response to selective β_2-AR stimulation. The results of selective stimulation of β_1-AR and β_2-AR in neonatal cardiac myocytes prepared from wild-type and AC5-knockout mice were also consistent with the idea that β_1-AR selectively couples with AC5. We believe these results are helpful for understanding the mechanisms underlying the different roles of AR subtypes in healthy and diseased hearts.

1. Introduction

Myocardial β-adrenergic receptors (β-AR) show developmentally specific subtype expression: for example, in rats, β_1-AR is the predominant adult isoforms (β_1 vs. β_2 59% vs. 41%), whereas β_2-AR is more highly expressed in the neonate (β_1 vs. β_2 36% vs. 64%) [1]. Thus, in adults under normal physiological conditions, catecholamine actions are mediated predominantly by β_1-AR acting via the Gsα-adenylyl cyclase (AC) pathway; on the other hand, the contribution of β_2-AR to catecholamine responsiveness is most prominent in neonatal ventricle, which lacks sympathetic innervation, and in failing/aged hearts, in which β_1-AR is selectively down-regulated. More importantly, chronic stimulation of β_1-AR and β_2-AR elicits opposing effects on cardiac myocytes [2]. Chronic β_1-AR stimulation by elevated plasma catecholamines and subsequent activation of the Gsα-AC-cyclic AMP (cAMP)-dependent signal transduction pathway play a crucial role in the development of heart failure [1,3]. Conversely, β_2-AR couples concurrently to Gsα and Giα, and activates cell survival pathways. Over the past decade, compelling evidence has accumulated that β_2-AR-Giα mediates a powerful cell survival pathway through activation of phosphatidylinositol 3-kinase (PI3-K)/Akt signaling in the heart [2,4–6]. However, the role of β_2-AR-Gsα in cell survival remains poorly understood.

AC is a membrane-bound enzyme that catalyzes the conversion of ATP to cAMP [7,8]. At least 10 isoforms are known [7,9,10], of which 7 are expressed in the heart, although type 5 (AC5) and type 6 (AC6) are the major AC isoforms in the heart [8,11]. Both are calcium (Ca^{2+})- and Gi-inhibitable and share most, if not all, of their biochemical properties [7,9,12]. AC5 was shown to be an adult isoform, whereas AC6 is more highly expressed in the neonate in

* Corresponding author. Department of Physiology, Tsurumi University School of Dental Medicine, 2-1-2 Tsurumi, Tsurumi-ku, Yokohama 230-8501, Japan. Fax: +81 45 585 2889.
** Corresponding author. Cardiovascular Research Institute, Yokohama City University Graduate School of Medicine, 3-9 Fukuura, Kanazawa-ku, Yokohama 236-0004, Japan. Fax: +81 45 788 1470.
E-mail addresses: okumura-s@tsuruni-u.ac.jp (S. Okumura), yishikaw@yokohama-cu.ac.jp (Y. Ishikawa).

http://dx.doi.org/10.1016/j.bbrc.2015.01.149
0006-291X/

rats [1,8,13,14]. We have previously demonstrated that disruption of AC5 did not alter the expression of β-AR/Gsα/AC/protein kinase A, but significantly inhibited both myocyte apoptosis and development of heart failure in response to chronic catecholamine or pressure-overload stress [11,15]. Conversely, disruption of AC6 promoted the development of myocyte apoptosis and heart failure in response to chronic catecholamine or pressure-overload stress [16–18].

Considering these findings, together with the facts that chronic β_1-AR stimulation plays an important role in the pathogenesis of heart failure, while chronic β_2 stimulation promotes cell survival, in addition to activating PI3-K/Akt signaling via Gi [5,6,19], we hypothesized that β_1-AR couples preferentially to AC5. Here, we examined this idea by means of both pharmacological and genetic studies in cardiac myocytes.

2. Materials and methods

2.1. Reagents

All chemicals were purchased from Sigma–Aldrich, except trypsin 1:250 (Difco), ITS (insulin-transferrin-selenium; GIBCO), [^{3}H]adenine (GE Healthcare), trichloroacetic acid (Wako) and 4′,6-diamidino-2-phenylindole,dihydrochloride (DAPI; Molecular Probes).

2.2. Myocyte preparation

Primary cultures of neonatal mouse cardiomyocytes were prepared from the heart of a 1-day-old mouse, as described previously with some modifications [20,21]. Briefly, cardiomyocytes were obtained by trypsinization and collagenization, and maintained at 37 °C in humidified air containing with 5% CO_2. To reduce the number of contaminating non-myocytes, dissociated cells were preplated on 100-mm culture dishes in minimum essential medium with 10% fetal bovine serum (FBS) containing 1% penicillin-streptomycin for 2 h. The nonattached cardiomyocyte-rich fraction was plated on plastic dishes. The culture medium was changed 24 h after seeding to minimum essential medium containing ITS with 1% penicillin-streptomycin.

2.3. [^{3}H]Adenine labeling and cAMP accumulation assay

Assay of cAMP accumulation assays in neonatal myocytes was performed with [^{3}H]adenine as described previously with some modifications [21,22]. Briefly, the cells were incubated with [^{3}H] adenine (3 μCi/well) for 24 h in humidified air containing 5% CO_2. Cells were washed three times with 20 mM HEPES-balanced serum-free minimum essential medium and incubated for 20 min at 37 °C, then pretreated with the same medium containing 0.5 mM IBMX with/without 10^{-7} M ICI118.551/10^{-7} M CGP20712A for 15 min at room temperature (RT). Reactions were started by the addition of isoproterenol (ISO) with/without dd-Ado (5 μM) for 5 min at RT and terminated by the addition of 12% (w/v) trichloroacetic acid, 0.25 mM ATP, and 0.25 mM cAMP. [^{3}H]ATP and [^{3}H]cAMP were separated on acidic alumina as described previously [23]. The cAMP production was calculated as [^{3}H]cAMP/([^{3}H] cAMP+[^{3}H]ATP) × 10^4.

2.4. Terminal transferase dUTP nick endlabeling (TUNEL) staining

In situ labeling of fragmented DNA in cardiomyocytes was performed with a TACS 2-Tdt Blue Apotosis Detection kit (Trevigen, Inc.) according to the manufacturer's instructions, as described previously by us and other groups [21,24,25].

2.5. Statistical analysis

Data were expressed as means ± SEM. The statistical significances of differences in cAMP accumulation in cardiac myocytes (Figs. 1 and 3A) and TUNNEL-positive cardiac myocytes (Figs. 2 and 3B) was determined by one-way ANOVA with Tukey's test. The criterion of significance was taken as $P < 0.05$.

3. Results

3.1. Effect of ICI118.551 or CGP20712A on ISO-promoted cAMP accumulation

We first examined the effects of ISO (10^{-8} to 10^{-6} M) on cAMP accumulation in neonatal cardiac myocytes in the presence and absence of 2′5′-dideoxyadenosine (dd-Ado; 5 μM), a specific AC5 inhibitor [21]. cAMP accumulation was significantly increased from baseline by ISO (10^{-7} or 10^{-6} M), but the magnitude of the increase was significantly suppressed (by approximately 29%) by dd-Ado (Fig. 1A).

We next examined the effect of pretreatment with ICI118.551 (10^{-7} M), a β_2-selective antagonist, on the ISO-promoted cAMP accumulations in neonatal cardiac myocytes (Fig. 1B). Under these conditions (β_1-selective stimulation), cAMP accumulation was significantly increased from baseline by ISO, and after ICI118.551 pretreatment the increase was approximately two-thirds of that in the absence of ICI118.551. The magnitude of the increase was significantly smaller (by approximately 39%) in the presence of dd-Ado.

We also examined the effect of pretreatment of CGP20712A (10^{-7} M), a β_1-selective antagonist, on the ISO-promote cAMP accumulation (Fig. 1C). Under these conditions (β_2-selective stimulation), cAMP accumulation was significantly increased from baseline by ISO (10^{-6} M), but the increase after CGP20712A pretreatment was only approximately one-third of that in the absence of CGP20712A (compare Fig. 1A). In this case, dd-Ado had no effect on the magnitude of the increase.

These data indicates that ISO-promoted cAMP accumulation is predominantly mediated by β_1-AR.

3.2. Effect of ICI118.551 or CGP20712A on ISO-mediated apoptosis of cardiac myocytes

ISO is known to induce cardiac apoptosis through the activation of β-AR, but the downstream regulatory mechanisms remains poorly understood [5,8,11,21,25]. We thus examined the mechanism of ISO-mediated cardiac apoptosis.

We first examined the effect of subtype-specific stimulation of β-AR on ISO-mediated cardiac apoptosis (Fig. 2). Cardiac apoptosis was significantly increased by approximately 1.5-fold from baseline by ISO (Baseline vs. ISO 14 ± 0.9 vs. 23 ± 0.2%, $P < 0.01$, $n = 4$). Pretreatment with ICI118.551 (10^{-7} M) did not significantly reduce ISO-mediated cardiac apoptosis (21 ± 0.8%, $n = 4$), whereas pretreatment with CGP20712A (10^{-7} M) completely suppressed it (11 ± 1.3%, $P < 0.01$ vs. ISO, $n = 4$). These data indicated that ISO-mediated cardiac apoptosis is mediated by activation of β_1-AR.

3.3. β_1-AR preferentially associates with AC5

We previously demonstrated that knockout of AC5 (AC5KO) decreased total AC activity by 30–40% in the mouse heart, but AC5KO was less susceptible to stresses, such as chronic ISO infusion or chronic pressure overload [8,11,12,21]. To confirm the results of pharmacological inhibition of AC5 with dd-Ado in cardiac myocytes (Fig. 1), we employed cardiac myocytes prepared from AC5KO.

Please cite this article in press as: T. Tsunematsu, et al., Coupling of β_1-adrenergic receptor to type 5 adenylyl cyclase and its physiological relevance in cardiac myocytes, Biochemical and Biophysical Research Communications (2015), http://dx.doi.org/10.1016/j.bbrc.2015.01.149

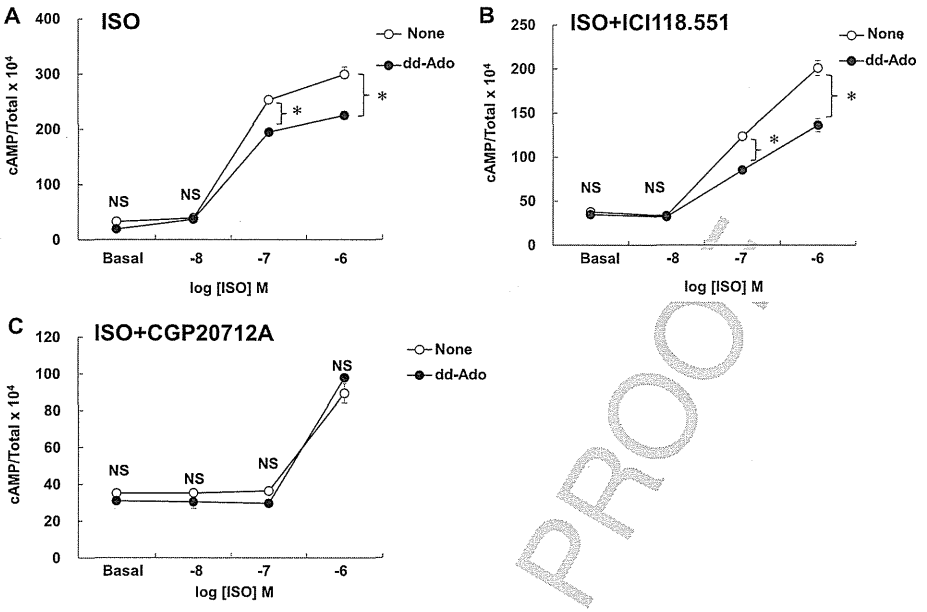

Fig. 1. Effects of AC5 inhibitor dd-Ado on cAMP accumulation in response to subtype-selective β-AR stimulation in cardiomyocytes. cAMP accumulation in neonatal cardiac myocytes treated with ISO (non-selective β-AR subtype stimulation) (A), ISO + ICI118.551 (10^{-7} M) (β_1-AR subtype selective stimulation) (B), or ISO + CGP20712A (10^{-7} M) (β_2-AR subtype selective stimulation) (C) was evaluated in the presence and absence of dd-Ado (5 μM), a selective AC5 inhibitor. cAMP accumulation induced by ISO (10^{-7} or 10^{-6} M) or ISO (10^{-7} or 10^{-6}) + ICI118.551 (10^{-7} M) was significantly decreased by dd-Ado, but no inhibitory effect was observed in the case of ISO + CGP20712A ($n = 5–6$, $P < 0.01$).

We first examined the effects of ISO (10^{-6} M) on cAMP accumulation in neonatal cardiac myocytes prepared from WT and AC5KO. cAMP accumulation was increased from baseline by ISO in both WT and AC5KO myocytes, but the increase was significantly suppressed in AC5KO myocytes (by approximately 26% versus WT, $P < 0.01$).

We next examined the effects of ICI118.551 (10^{-7} M) and CGP20712A (10^{-7} M) on ISO (10^{-6} M)-promoted cAMP accumulation in cardiac myocytes. cAMP accumulation was reduced by approximately 26% and 43% by ICI118.551 pretreatment in WT and AC5KO myocytes, respectively. However, CGP20712A pretreatment reduced cAMP accumulation to the baseline level (Fig. 3A).

We also examined the effects of ISO on cardiac apoptosis in WT and AC5KO myocytes by TUNEL staining. The number of TUNEL-positive cardiac myocytes was increased by 1.6-fold from baseline in WT myocytes, but this increase was blocked in AC5KO myocytes, in the presence or absence of ICI118.551 or CGP20712A (Fig. 3B).

Since AC5 is known to play an important role in cardiac apoptosis [8,11,21], these data support the idea that β_1-AR is coupled preferentially to AC5.

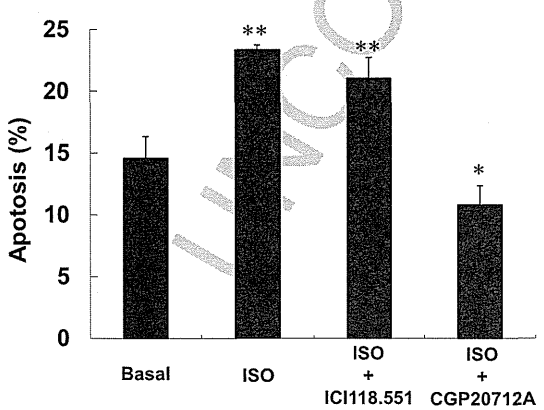

Fig. 2. Apoptosis induced by subtype-selective β-AR stimulation. Induction of TUNEL-positive cardiomyocytes in response to subtype-selective β-AR stimulation: ISO (non-selective β-AR subtype stimulation), ISO (10^{-6} M) + ICI118.551 (10^{-7} M) (β_1-AR subtype selective stimulation) or ISO (10^{-6} M) + CGP20712A (10^{-7} M) (β_2-AR subtype selective stimulation) (*$P < 0.05$, **$P < 0.01$, *NS*, not significant, $n = 4$).

4. Discussion

In order to examine the mechanism underlying the opposing effects of β_1-AR and β_2-AR on cardiac myocytes [2], we adopted two approaches. Firstly, we examined the effects of dd-Ado, a specific AC5 inhibitor [21] on cAMP accumulation and cardiac apoptosis induced by ISO under conditions of selective β_1-AR or β_2-AR stimulation. Secondly, we examined cAMP accumulation and cardiac apoptosis using cardiac myocytes from AC5KO under conditions of selective β_1-AR or β_2-AR stimulation. Both approaches indicated that cAMP accumulation and cardiac apoptosis in response to selective β_1-AR stimulation were significantly suppressed by inhibition or knockout of AC5, whereas no decrease was observed in the case of selective β_2-AR stimulation. These results are consistent with our hypothesis that β_1-AR associates preferentially with AC5.

Caveolin-3, a major subtype in the heart, acts as a scaffolding protein by direct interaction with and modulation of the activity of G-protein-coupled receptor signaling components [26]. We and other groups have reported colocalization of caveolin-3 with G-protein-coupled receptor signaling components including β_1-AR, β_2-AR, and AC5/6 in cardiac myocytes [27–29]. However, caveolin-3 is distributed in both surface sarcolemma and long membrane invaginations known as transverse tubules (t-tubules) in cardiac myocytes [30]. More recently, subtype-specific subcellular distribution of β-AR and cardiac AC isoforms (AC5/6) within the plasma membrane was demonstrated by means of electrophysiological techniques: AC5 is localized mainly at t-tubules and AC6 is localized at surface sarcolemma, whereas β_1-AR is localized at t-tubules and

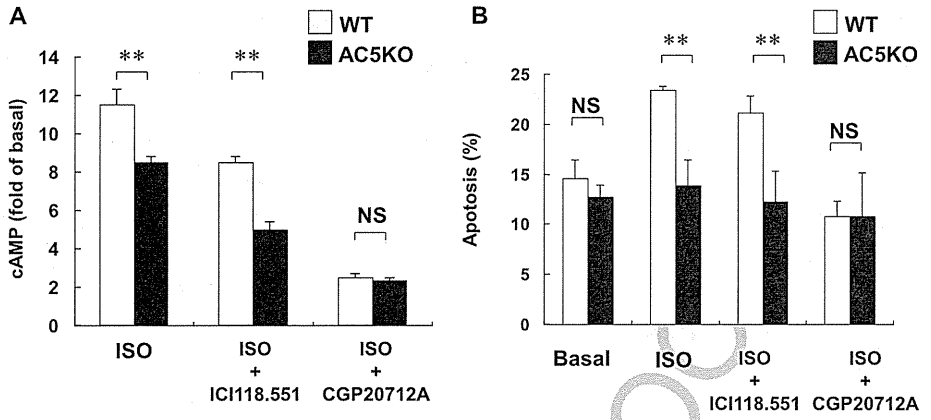

Fig. 3. cAMP accumulation and apoptosis in AC5KO myocytes in response to subtype-selective β-AR stimulation. (A) cAMP accumulation in neonatal cardiac myocytes was compared between AC5KO and WT myocytes treated with ISO (10^{-6} M) (non-selective β-AR subtype stimulation), ISO (10^{-6} M) + ICI118.551 (10^{-7} M) (β_1-AR subtype selective stimulation), or ISO (10^{-6} M) + CGP20712A (10^{-7} M) (β_2-AR subtype selective stimulation). $^{**}P < 0.01$, $n = 4$. (B) Induction of apoptosis in AC5KO and WT myocytes was evaluated by TUNEL staining. The number of TUNEL-positive cardiac myocytes was increased 1.6-fold from baseline in ISO-treated WT myocytes, but the increase was suppressed in AC5KO myocytes, independently of the presence or absence of ICI118.551 or CGP20712A. $^{**}P < 0.01$, *NS*, not significant, $n = 4$–6.

surface sarcolemma and β_2-AR is localized only at surface sarcolemma [31,32]. These findings, together with the data obtained in the present study, may suggest that β_1-AR preferentially couples with AC5 at t-tubules, while β_2-AR might preferentially couple with AC6 at surface sarcolemma, and these subtype-specific couplings of β-AR and cardiac AC isoforms might account for opposing effects of β_1/β_2-AR and AC5/6 on cardiac myocytes [2]. Our present findings represent the first evidence in support of this explanation of the differential regulation and functionality of β-AR subtypes in healthy and diseased hearts.

Conflict of interest

Q3 None.

Acknowledgments

This study was supported in part by grants from the Ministry of Health, Labor and Welfare (Dr. Ishikawa), a Grant-in-Aid for Scientific Research on Innovative Areas (22136009), and grants from Q4 the Japanese Ministry of Education, Culture, Sports, Science, and Technology (Drs. Ishikawa, Okumura, Fujita, Sato, Yokoyama, Q5 Mototani), National Cerebral and Cardiovascular Center (Dr. Ishi- Q6,7 kawa), Takeda Science Foundation (Dr. Okumura), Yokohama Foundation for Advancement of Medical Science (Dr. Okumura), Q8,9 Yokohama Academic Foundation (Dr. Ohnuki), Research Foundation Q10 for Community Medicine (Dr. Okumura), and Suzuken Memorial Foundation (Dr. Okumura).

References

[1] C. Morisco, D.C. Zebrowski, D.E. Vatner, S.F. Vatner, J. Sadoshima, β-adrenergic cardiac hypertrophy is mediated primarily by the β_1-subtype in the rat heart, J. Mol. Cell. Cardiol. 33 (2001) 561–573.
[2] M. Zheng, W. Zhu, Q. Han, R.P. Xiao, Emerging concepts and therapeutic implications of β-adrenergic receptor subtype signaling, Pharmacol. Ther. 108 (2005) 257–268.
[3] G. Lewin, M. Matus, A. Basu, K. Frebel, S.P. Rohsbach, A. Safronenko, M.D. Seidl, F. Stumpel, I. Buchwalow, S. Konig, S. Engelhardt, M.J. Lohse, W. Schmitz, F.U. Muller, Critical role of transcription factor cyclic AMP response element modulator in β_1-adrenoceptor-mediated cardiac dysfunction, Circulation 119 (2009) 79–88.
[4] G. Fajardo, M. Zhao, T. Urashima, S. Farahani, D.Q. Hu, S. Reddy, D. Bernstein, Deletion of the β_2-adrenergic receptor prevents the development of cardiomyopathy in mice, J. Mol. Cell. Cardiol. 63 (2013) 155–164.
[5] Y. Ohnuki, D. Umeki, Y. Mototani, H. Jin, W. Cai, K. Shiozawa, K. Suita, Y. Saeki, T. Fujita, Y. Ishikawa, S. Okumura, Role of cyclic amp sensor Epac1 in masseter muscle hypertrophy and myosin heavy chain transition induced by β_2-adrenoceptor stimulation, J. Physiol. 592 (2014) 5461–5475.
[6] D. Umeki, Y. Ohnuki, Y. Mototani, K. Shiozawa, T. Fujita, Y. Nakamura, Y. Saeki, S. Okumura, Effects of chronic Akt/mTOR inhibition by rapamycin on mechanical overload-induced hypertrophy and myosin heavy chain transition in masseter muscle, J. Pharmacol. Sci. 122 (2013) 278–288.
[7] Y. Ishikawa, C.J. Homcy, The adenylyl cyclases as integrators of transmembrane signal transduction, Circ. Res. 80 (1997) 297–304.
[8] S. Okumura, S. Suzuki, Y. Ishikawa, New aspects for the treatment of cardiac diseases based on the diversity of functional controls on cardiac muscles: effects of targeted disruption of the type 5 adenylyl cyclase gene, J. Pharmacol. Sci. 109 (2009) 354–359.
[9] J. Hanoune, N. Defer, Regulation and role of adenylyl cyclase isoforms, Annu Rev. Pharmacol. Toxicol. 41 (2001) 145–174.
[10] C. Steegborn, Structure, mechanism, and regulation of soluble adenylyl cyclases - similarities and differences to transmembrane adenylyl cyclases, Biochim. Biophys. Acta (2014). Q11
[11] S. Okumura, G. Takagi, J. Kawabe, G. Yang, M.C. Lee, C. Hong, J. Liu, D.E. Vatner, J. Sadoshima, S.F. Vatner, Y. Ishikawa, Disruption of type 5 adenylyl cyclase gene preserves cardiac function against pressure overload, Proc. Natl. Acad. Sci. U S A 100 (2003) 9986–9990.
[12] S. Okumura, J. Kawabe, A. Yatani, G. Takagi, M.C. Lee, C. Hong, J. Liu, I. Takagi, J. Sadoshima, D.E. Vatner, S.F. Vatner, Y. Ishikawa, Type 5 adenylyl cyclase disruption alters not only sympathetic but also parasympathetic and calcium-mediated cardiac regulation, Circ. Res. 93 (2003) 364–371.
[13] K. Tobise, Y. Ishikawa, S.R. Holmer, M.J. Im, J.B. Newell, H. Yoshie, M. Fujita, E.E. Susannie, C.J. Homcy, Changes in type VI adenylyl cyclase isoform expression correlate with a decreased capacity for cAMP generation in the aging ventricle, Circ. Res. 74 (1994) 596–603.
[14] I. Espinasse, V. Iourgenko, N. Defer, F. Samson, J. Hanoune, J.J. Mercadier, Type V, but not type VI, adenylyl cyclase mRNA accumulates in the rat heart during ontogenic development. Correlation with increased global adenylyl cyclase activity, J. Mol. Cell. Cardiol. 27 (1995) 1789–1795.
[15] S. Okumura, D.E. Vatner, R. Kurotani, Y. Bai, S. Gao, Z. Yuan, K. Iwatsubo, C. Ulucan, J. Kawabe, K. Ghosh, S.F. Vatner, Y. Ishikawa, Disruption of type 5 adenylyl cyclase enhances desensitization of cyclic adenosine monophosphate signal and increases Akt signal with chronic catecholamine stress, Circulation 116 (2007) 1776–1783.
[16] T. Tang, M.H. Gao, N.C. Lai, A.L. Firth, T. Takahashi, T. Guo, J.X. Yuan, D.M. Roth, H.K. Hammond, Adenylyl cyclase type 6 deletion decreases left ventricular function via impaired calcium handling, Circulation 117 (2008) 61–69.
[17] T. Tang, N.C. Lai, H.K. Hammond, D.M. Roth, Y. Yang, T. Guo, M.H. Gao, Adenylyl cyclase 6 deletion reduces left ventricular hypertrophy, dilation, dysfunction, and fibrosis in pressure-overloaded female mice, J. Am. Coll. Cardiol. 55 (2010) 1476–1486.
[18] T. Tang, N.C. Lai, A.T. Wright, M.H. Gao, P. Lee, T. Guo, R. Tang, A.D. McCulloch, H.K. Hammond, Adenylyl cyclase 6 deletion increases mortality during sustained β-adrenergic receptor stimulation, J. Mol. Cell. Cardiol. 60 (2013) 60–67.
[19] Y. Ohnuki, D. Umeki, W. Cai, N. Kawai, Y. Mototani, K. Shiozawa, H.L. Jin, T. Fujita, E. Tanaka, Y. Saeki, S. Okumura, Role of masseter muscle β_2-adrenergic signaling in regulation of muscle activity, myosin heavy chain transition, and hypertrophy, J. Pharmacol. Sci. 123 (2013) 36–46.

[20] N. Nyui, K. Tamura, K. Mizuno, T. Ishigami, K. Hibi, M. Yabana, M. Kihara, A. Fukamizu, H. Ochiai, S. Umemura, K. Murakami, S. Ohno, M. Ishii, Stretch-induced MAP kinase activation in cardiomyocytes of angiotensinogen-deficient mice, Biochem. Biophys. Res. Commun. 235 (1997) 36–41.
[21] K. Iwatsubo, S. Minamisawa, T. Tsunematsu, M. Nakagome, Y. Toya, J.E. Tomlinson, S. Umemura, R.M. Scarborough, D.E. Levy, Y. Ishikawa, Direct inhibition of type 5 adenylyl cyclase prevents myocardial apoptosis without functional deterioration, J. Biol. Chem. 279 (2004) 40938–40945.
[22] Y. Toya, C. Schwencke, Y. Ishikawa, Forskolin derivatives with increased selectivity for cardiac adenylyl cyclase, J. Mol. Cell. Cardiol. 30 (1998) 97–108.
[23] T. Onda, Y. Hashimoto, M. Nagai, H. Kuramochi, S. Saito, H. Yamazaki, Y. Toya, I. Sakai, C.J. Homcy, K. Nishikawa, Y. Ishikawa, Type-specific regulation of adenylyl cyclase. Selective pharmacological stimulation and inhibition of adenylyl cyclase isoforms, J. Biol. Chem. 276 (2001) 47785–47793.
[24] X. Long, M.T. Crow, S.J. Sollott, L. O'Neill, D.S. Menees, M. de Lourdes Hipolito, M.O. Boluyt, T. Asai, E.G. Lakatta, Enhanced expression of p53 and apoptosis induced by blockade of the vacuolar proton ATPase in cardiomyocytes, J. Clin. Invest. 101 (1998) 1453–1461.
[25] S. Okumura, T. Fujita, W. Cai, M. Jin, I. Namekata, Y. Mototani, H. Jin, Y. Ohnuki, Y. Tsuneoka, R. Kurotani, K. Suita, Y. Kawakami, S. Hamaguchi, T. Abe, H. Kiyonari, T. Tsunematsu, Y. Bai, S. Suzuki, Y. Hidaka, M. Umemura, Y. Ichikawa, U. Yokoyama, M. Sato, F. Ishikawa, H. Izumi-Nakaseko, S. Adachi-Akahane, H. Tanaka, Y. Ishikawa, *Epac1*-dependent phospholamban phosphorylation mediates the cardiac response to stresses, J. Clin. Invest. 124 (2014) 2785–2801.
[26] C. Schwencke, R.C. Braun-Dullaeus, C. Wunderlich, R.H. Strasser, Caveolae and caveolin in transmembrane signaling: implications for human disease, Cardiovasc Res. 70 (2006) 42–49.
[27] C. Schwencke, S. Okumura, M. Yamamoto, Y.J. Geng, Y. Ishikawa, Colocalization of β-adrenergic receptors and caveolin within the plasma membrane, J. Cell. Biochem. 75 (1999) 64–72.
[28] C. Schwencke, M. Yamamoto, S. Okumura, Y. Toya, S.J. Kim, Y. Ishikawa, Compartmentation of cyclic adenosine 3′,5′-monophosphate signaling in caveolae, Mol. Endocrinol. 13 (1999) 1061–1070.
[29] R.S. Ostrom, J.D. Violin, S. Coleman, P.A. Insel, Selective enhancement of β-adrenergic receptor signaling by overexpression of adenylyl cyclase type 6: colocalization of receptor and adenylyl cyclase in caveolae of cardiac myocytes, Mol. Pharmacol. 57 (2000) 1075–1079.
[30] B.P. Head, H.H. Patel, D.M. Roth, N.C. Lai, I.R. Niesman, M.G. Farquhar, P.A. Insel, G-protein-coupled receptor signaling components localize in both sarcolemmal and intracellular caveolin-3-associated microdomains in adult cardiac myocytes, J. Biol. Chem. 280 (2005) 31036–31044.
[31] C. Cros, F. Brette, Functional subcellular distribution of β_1- and β_2-adrenergic receptors in rat ventricular cardiac myocytes, Physiol. Rep. (2013) e00038.
[32] V. Timofeyev, R.E. Myers, H.J. Kim, R.L. Woltz, P. Sirish, J.P. Heiserman, N. Li, A. Singapuri, T. Tang, V. Yarov-Yarovoy, E.N. Yamoah, H.K. Hammond, N. Chiamvimonvat, Adenylyl cyclase subtype-specific compartmentalization: differential regulation of L-type Ca^{2+} current in ventricular myocytes, Circ. Res. 112 (2013) 1567–1576.

Please cite this article in press as: T. Tsunematsu, et al., Coupling of β_1-adrenergic receptor to type 5 adenylyl cyclase and its physiological relevance in cardiac myocytes, Biochemical and Biophysical Research Communications (2015), http://dx.doi.org/10.1016/j.bbrc.2015.01.149

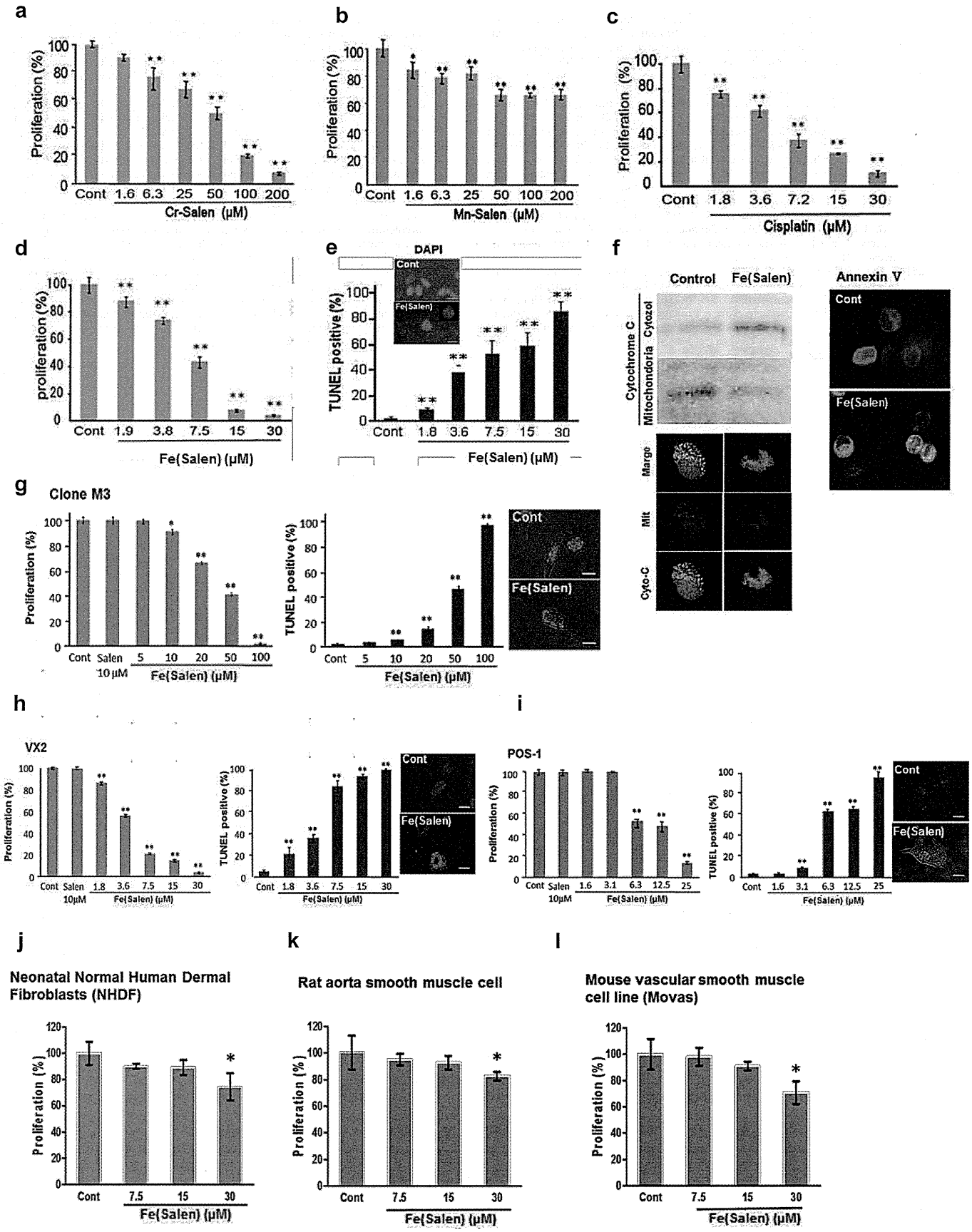
a
Proliferation (%)
Cont 1.6 6.3 25 50 100 200
Cr-Salen (μM)
b
Proliferation (%)
Cont 1.6 6.3 25 50 100 200
Mn-Salen (μM)
c
Proliferation (%)
Cont 1.8 3.6 7.2 15 30
Cisplatin (μM)
d
proliferation (%)
Cont 1.9 3.8 7.5 15 30
Fe(Salen) (μM)
e
DAPI
Cont
Fe(Salen)
TUNEL positive (%)
Cont 1.8 3.6 7.5 15 30
Fe(Salen) (μM)
f
Control
Fe(Salen)
Annexin V
Cytochrome C
Cytozol
Mitochondoria
Cont
Fe(Salen)
Marge
Mit
Cyto-C
g
Clone M3
Proliferation (%)
Cont Salen 10 μM 5 10 20 50 100
Fe(Salen) (μM)
TUNEL positive (%)
Cont 5 10 20 50 100
Fe(Salen) (μM)
Cont
Fe(Salen)
h
VX2
Proliferation (%)
Cont Salen 10μM 1.8 3.6 7.5 15 30
Fe(Salen) (μM)
TUNEL positive (%)
Cont 1.8 3.6 7.5 15 30
Fe(Salen) (μM)
Cont
Fe(Salen)
i
POS-1
Proliferation (%)
Cont Salen 10μM 1.6 3.1 6.3 12.5 25
Fe(Salen) (μM)
TUNEL positive (%)
Cont 1.6 3.1 6.3 12.5 25
Fe(Salen) (μM)
Cont
Fe(Salen)
j
Neonatal Normal Human Dermal Fibroblasts (NHDF)
Proliferation (%)
Cont 7.5 15 30
Fe(Salen) (μM)
k
Rat aorta smooth muscle cell
Proliferation (%)
Cont 7.5 15 30
Fe(Salen) (μM)
l
Mouse vascular smooth muscle cell line (Movas)
Proliferation (%)
Cont 7.5 15 30
Fe(Salen) (μM)

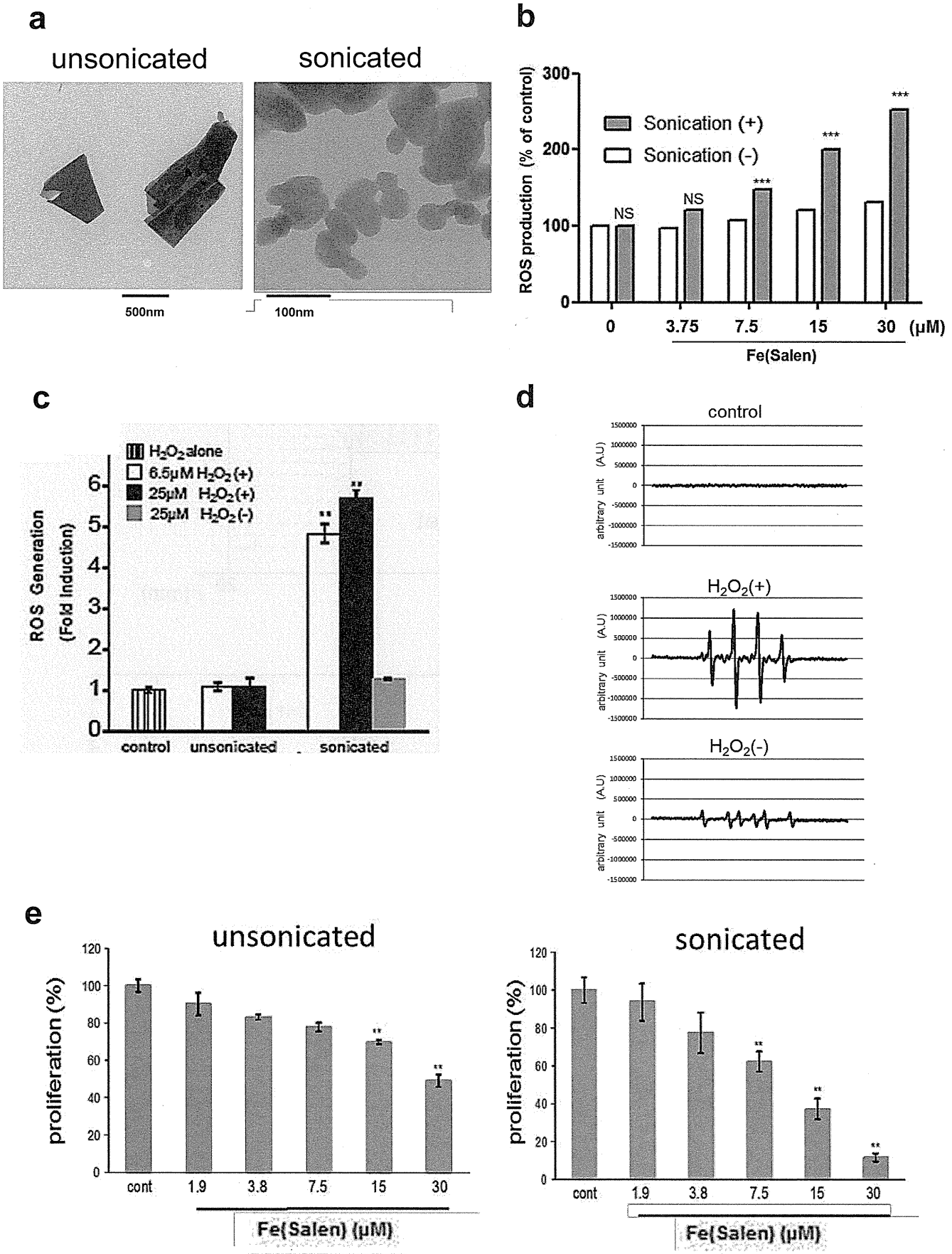
a
unsonicated
sonicated
500nm
100nm
b
ROS production (% of control)
Sonication (+)
Sonication (-)
NS
NS
***
***
***
0
3.75
7.5
15
30
(μM)
Fe(Salen)
c
ROS Generation (Fold Induction)
H2O2 alone
6.5μM H2O2(+)
25μM H2O2(+)
25μM H2O2(-)
control
unsonicated
sonicated
d
control
H2O2(+)
H2O2(-)
arbitrary unit (A.U)
e
unsonicated
sonicated
proliferation (%)
cont
1.9
3.8
7.5
15
30
Fe(Salen) (μM)